ALMA MATER STUDIORUM A.D. 1088
UNIVERSITÀ DI BOLOGNA

DIPARTIMENTO DI SCIENZE BIOLOGICHE, GEOLOGICHE E AMBIENTALI

Corso di Laurea Magistrale in Geologia e Territorio

Curriculum *Raw Materials Exploration and Sustainability*

Tesi di Laurea Magistrale

Graphite for lithium-ion batteries: mineral analysis and global Material Flow Analysis

Candidato:
Sofia Genovesi

Relatore:
Prof. Paolo S. Garofalo

Correlatore:
Prof. Daniel Beat Muller
Dott. Romain Guillaume Billy
Dott. Fernando Aguilar Lopez

Sessione Maggio 2022
Anno Accademico 2020-2021

Abstract

Graphite is a mineral commodity used as anode for lithium-ion batteries (LIBs), and its global demand is doomed to increase significantly in the future due to the forecasted global market demand of electric vehicles. Currently, the graphite used to produce LIBs is a mix of synthetic and natural graphite. The first one is produced by the crystallization of petroleum by-products and the second comes from mining, which causes threats related to pollution, social acceptance, and health. This MSc work has the objective of determining compositional and textural characteristics of natural, synthetic, and recycled graphite by using SEM-EDS, XRF, XRD, and TEM analytical techniques and couple these data with dynamic Material Flow Analysis (MFA) models, which have the objective of predicting the future global use of graphite in order to test the hypothesis that natural graphite will no longer be used in the LIB market globally. The mineral analyses reveal that the synthetic graphite samples contain less impurities than the natural graphite, which has a rolled internal structure similar to the recycled one. However, recycled graphite shows fractures and discontinuities of the graphene layers caused by the recycling process, but its rolled internal structure can help the Li-ions' migration through the fractures. Three dynamic MFA studies have been conducted to test distinct scenarios that include graphite recycling in the period 2022-2050 and it emerges that - irrespective of any considered scenario - there will be an increase of synthetic graphite demand, caused by the limited stocks of battery scrap available. Hence, I conclude that both natural and recycled graphite is doomed to be used in the LIB market in the future, at least until the year 2050 when the stock of recycled graphite production will be enough to supersede natural graphite. In addition, some new improvement in the dismantling and recycling processes are necessary to improve the quality of recycled graphite.

Keywords: Graphite, Graphite recycling, Material Flow Analysis, Anode materials, Li-ion battery, Electric vehicles

Contents

1. Introduction

Greenhouse gases, CO_2, CH_4, N_2O, and fluorinated gases, are the principal contributors of the global warming because of the greenhouse effect that they cause, which is the interaction between Sun's energy and the greenhouse gases that capture heat (*Kweku et al., 2018*). From the Paris Agreement of 2015, the United Nations Framework Convention on Climate Change decided to stipulate article 2 point 1.b, in which they declare that they will try to "Holding the increase in the global average temperature to well below 2°C above pre-industrial levels and pursuing efforts to limit the temperature increase to 1.5°C above pre-industrial levels, recognizing that this would significantly reduce the risks and impacts of climate change" (United Nations, 2015). In 2020, the average global surface temperature was 1.19° C warmer than the pre-industrial period. In 2021, the temperature was +0.85C, but this data could be affected by the pandemic historical period (*NOAA National Centers for Environmental information, 2022*). From the European Union, the principal causes of greenhouse gases emissions and thus global warming are deforestation, increase of livestock farming, use of fertilisers containing nitrogen, fluorinated gases, and burning of coal, oil, and gas *(European Commission, 2015)*. This last cause is related with the continental inputs from industries and vehicles, which burn fossil fuels for a number of activities. For this reason, the production of electric vehicles, and thus that of lithium-ion batteries (LIBs) for domestic electric vehicles (EVs), is estimated to grow significantly in the next decades.

The anodes for EVs' LIBs are essentially made of a mixture of equal proportions (50%) of natural and synthetic graphite. Natural graphite is mined and treated to remove impurities, while the synthetic graphite is produced by the crystallization (graphitization) process applied to by-products of petroleum refinery, namely the as calcined green coke and calcined needle coke .The motivation behind the mixing of these two types of graphite lies in the fact that the price of natural graphite is lower than that of the synthetic one (i.e., 6000-10000 as opposed to 20.000 $/tonne) (e.g. *West Water Resources, 2021* and *Canada Carbon, 2022*). Another reason is the purity of the synthetic graphite, which is higher than that of the natural graphite. According to Robinson et al. (2017), data show that synthetic graphite can reach 99.9% of carbon content while the natural one ranges between 75 and 98% . Based on the considerations above, taking into account that on average each passenger electric vehicle contains 70kg of graphite (*Northern Graphite Corporation, 2022*), there will be about 35kg of synthetic graphite in each future vehicle if industry

production follows the business as usual. As a result of this, the domestic EV market will be closely dependent on the mining and petroleum extraction, which is a blatant contradiction with respect to the objectives of the green transition.

At the global scale, about 95% of the graphite mines are open pit and the remaining 5% are underground mines (*Handl, 2021, see also Table 1*). The current global reserves of natural graphite are 320.000.000 Mt. and China is the largest producer of natural graphite even if its reserves are not the largest in the world. However, it is noteworthy that data could change in the future because new extraction sites could be found.

Table 1. Current natural graphite production and reserves, data from USGS, 2022.

	Reserves		Producers	
No.	Nation	Mt	Nation	Mt in 2021
1st	Turkey	90.000.000	China	820.000
2nd	China	73.000.000	Brazil	68.000
3rd	Brazil	70.000.000	Mozambique	30.000
4th	Madagascar	26.000.000	Russia	27.000
5th	Mozambique	25.000.000	Madagascar	22.000
6th	Tanzania	18.000.000	Ukraine	17.000

Mining and purification processes of natural graphite cause health, and environmental damages in the areas surrounding the mine activities, which impacts the social acceptance of this industry. A relevant example is provided by the reactions of the population of the Chinese villages of Laixi, Jidong, and Mashan, in which natural graphite plants were set up. These are the main natural graphite plants of that Chinese province. Media reports on these Chinese locations (*Whoriskey et al., 2016*) showed that since the start of graphite production in these plants, the graphite powder was visible in the air, covered buildings, crops, polluted water, and killed trees. It was also demonstrated an increase of several heart and respiratory cases in all these Chinese villages, showing that a social health problem is related to this industry, which generates a potentially big sustainability problem.

In addition to the issues listed above, another aspect to consider to evaluate the sustainability of the present day graphite industry is the fact that the purification of natural graphite has an efficiency of ca.50% from mining to the end-product.

Previous studies on the lithium-ion batteries of electric vehicles used material flow analysis and dynamic material flow analysis to evaluate the cumulative demand up to 2050 of Li, Co, Ni, and Mn (*Kamran et al., 2021*). A specific objective was understanding the potential of circularity of cathode materials (*Dunn et al., 2021*) and study the LIBs' raw materials flow up to 2040 including recycling (*Abdelbaky et al., 2021*). Unfortunately, none of these studies focused on graphite and its recycling. In contrast, some mineral analysis aimed at evaluating graphite recycling from LIBs (*Rothermel et al., 2016*) and synthetic and natural graphite (*e.g., Ishii et al., 2017*) identified trace amounts of edge sites of natural graphite, synthetic graphite, and high-T treated coke.

The anode production for the LIBs of electric vehicles consists in mixing natural graphite and synthetic graphite powders in equal quantities (50-50%). Synthetic graphite is artificial graphite produced by the crystallization of petroleum by-products of the oil industry such as needle coke and green coke, which are produced thanks to the delayed coking process of petroleum refinery residues. The involvement of synthetic graphite in the anode production implies an effective link between electric vehicle market and the oil industry. Considering the high probability of a large global demand of high-purity graphite to sustain the LIB industrial production, a quantitative study on the graphite industry is essential to evaluate the dependency of this industry on the two major supply sources –primary resources and oil industry. These quantitative evaluations are essential to guide the future national and trans-national policies on green energy and green policies.

In this thesis, I apply Material Flow Analysis (MFA) to improve the system understanding of global graphite production and use. With this approach I tentatively quantify world production and recycling in order to evaluate possible reduction of petroleum by-products, and substitution of mining. This is carried out by focussing on the following goals:

- Describe the structural, compositional, and morphological differences between natural, synthetic, and recycled graphite;
- Observe the steps before-during-after of recycled graphite production from a structural, chemical, and morphological point of views;
- Use this analysis to test the hypothesis (?), from technical and systemic points of view, that recycled graphite can replace the natural one;
- Suggest (?) a global system of graphite production, use, disposal, and recycling for the LIBs used in passenger electric vehicles;

- Define possible future scenarios of graphite for the EV LIBs up to 2050, trying to observe how graphite recycling can replace the natural graphite and change the synthetic graphite demand. This would have obvious effects on the coke demand.

2 Graphite material

2.1 Crystalline graphite

Graphite is the form of elemental carbon that crystallizes in the hexagonal system and is arranged in a layered, parallel-stacked form (*c*-axis). Each carbon hexagonal layer, when isolated, is called graphene (*a*-axis) (Fig. 1). The interplanar distance is 3.354 Å and the molecular layers are linked with the Van Der Waals forces, while the carbon atoms are linked with the three closest with the covalent bonds which causes a distance between them of 1.415 Å. *(Robinson et al., 2017; Khan et al., 2016).*

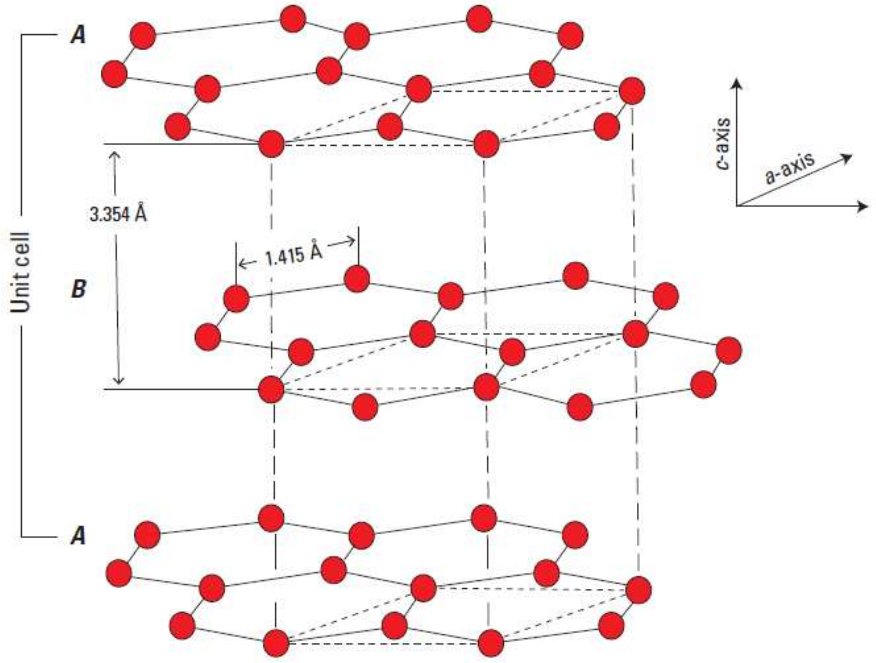

Figure 1. Atomic structure of graphite. Red points: carbon atoms, which forms the layered hexagonal structure. (From Robinson et al., 2017)

Graphite has a grey to black colour, it has a density comprised between 2.09 and 2.26 g/cm^3 because of structural imperfections such as porosity, lattice vacancies, and dislocations, and a melting point of 3550°C. This material is very important for its high heat and electric

conductivity, for its low thermal expansion, for its high thermal and corrosion resistance. (*Pierson, 1993).*

2.2 Graphite in nature

Graphite in nature can be found as a microcrystalline phase named “amorphous” and as crystalline flakes and veins. The “amorphous” graphite is compact and microcrystalline (grains size <4μm), and the ore appears in carbonaceous rocks as layers and lenses which can reach few meters of thickness and several km in length. The genesis can occur during contact metamorphism caused by intrusions onto sedimentary rocks rich in organic matter, and/or during regional metamorphism of carbonaceous sediments. The ore grade varies from 50 to 90% and after concentration/treatment, the carbon content (product grade) varies from 60 to 90%.

Flake graphite is well developed crystalline with a grain size between 40 μm and 4 cm, and it is formed from the regional metamorphism of carbonaceous sediments. The deposits are typically strata-bound, up to 33 m of thickness and km of length. The ore grade is variable from 5 to 30%, even if it is possible to have higher values, and the product grade is from 75 to 97%.

Vein graphite crystals are more developed compared to all other graphite specimens. Crystals can reach 10 cm and they interlock. The origin of these kind of epigenetic deposits is metamorphic due to high grade metamorphic rocks, which forms these veins. The orebody consists of veins and fracture-filling which follow or crosscut the metamorphic structures or the contacts with a thickness from 0.05 m to 3 m and a length up to hundreds of meters. The ore grade is from 40 to 90%, while the product grade is from 90 to 99.99% (*Fernley 2020*, *Robinson et al., 2017*).

2.3 Green coke and needle coke for synthetic graphite production

The starting products for the synthetic graphite production are petroleum by-products, calcined green coke and needle coke. In general, coke is produced by delayed coking of petroleum refinery residues, which consists of delayed coking of petroleum refinery residues. The delayed coking process is explained in Figure 2. The procedure starts with the feedstock which is directly inserted to the fractionator (a) and heated to remove lighter fractions (middle distillate, Fig.2), then the material is heated in the furnace (b) at temperature between 450 and 500°C that lead to the thermal cracking (b). The gases in the coking chamber (like naphtha and heavy coker gas oil) are lead to the fractionator for

separation. Successively, the heated feedstock enters in the coking drum (c) in which cracking reactions continue and the coking drum chamber cools down. When the coke stops its cracking reactions, the material is removed from the chamber by high pressure water cutting, which comes from the recovery of the already used water for the coke cutting. More specifically, the cutted coke goes through a crushing process (d) and then, the coke and the used water enter in a coke-water pit (g). From this tank, the coke is dewatered (e) and then, the dry coke is ready, while water is recovered in a water tank and used another time at high pressure to cut the nest coke batch (Sawarkar et al., 2007, and Predel, 2012).

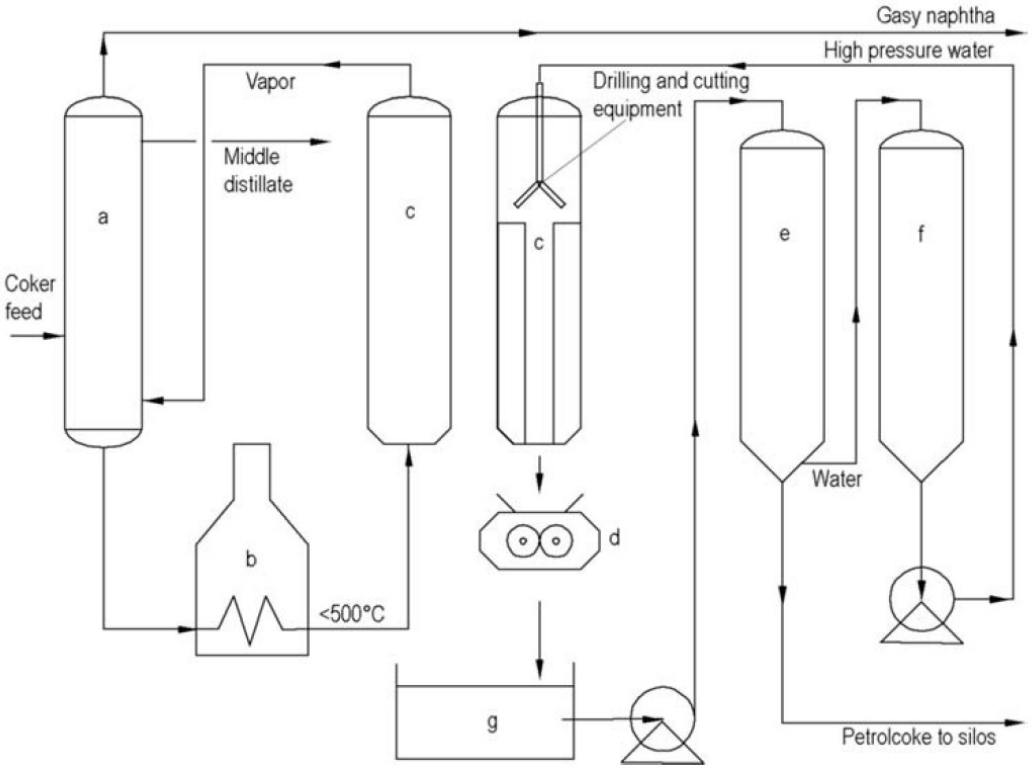

Figure 2. Flow sheet of delayed coking. a) Fractionator; b) Furnace; c) Coke drum; d) Crusher; e) Coke dewatering; f) Water tank; g) Coke-water pit (from Predel, 2012)

The delayed coking is the common passage between all types of coke, but if the purpose of the coke is to create synthetic graphite for anode, the produced coke (in this case petroleum green coke and needle coke) must be calcined. The calcination process can be performed even during coke treatment for synthetic graphite production, and it is essential to remove the hydrogen from the coke structure. This reaction is also called dehydrogenation, i.e. a conversion from hydrocarbon to elemental carbon (*Sawarkar et al.,*

2007). After this last process, the coke products will be regular calcined coke and calcined needle coke.

The difference between the calcined needle coke and the regular calcined coke is that the first one is produced with a feedstock with a lower sulphur and metal content (slurry oil and decan oil from catalytic cracking), and that during the delayed coking are required higher drum pressure and temperature (*Sawarkar et al., 2007*).

Needle coke is a premium-quality coke, it has a regular crystal with a needle-like structure of size between 4-5 nm. This coke quality shows several elliptical and interconnected pores, and from a chemical point of view, the quality is superior thanks the lower content of metals and sulphur (0.1-0.8 wt%, regular calcined coke: 1.0-3.0 wt%, *Sawarkar et al., 2007; Predel, 2012*).

Within petroleum, sulphur is may form organic C-S bonds, which have an extreme thermal stability. Therefore, S is difficult to remove during the delayed coking process. In addition, sulphur can break out during the calcination process: at a T of 1400-1500°C this element fractionates into the gas phase through the porosity of the needle- and green petroleum coke grains creating cracks. This phenomenon is called "puffing effect" and it could take place even during the graphitization process. The consequence is a substantial conductivity decrease due to the neo-formed graphite crystal cracking (*Sawarkar et al., 2007; Fujimoto et al., 1989*). Due to this process, according to *Sawarkar et al. (2007),* it is important that the coke used for synthetic graphite production has a sulphur content below 1.2 wt%. In case of higher concentrations, the electrode producer has to extend the time requirements of the graphitization to minimize the irreparable cracking.

2.4 Graphite pitch coating

Carbon pitch is frequently used for graphite anode material coating because of its positive effects on the conductivity: a uniform and isotropic protective layer around the graphite particles improves the conductivity and suppresses the reaction between the electrolyte and graphite (*Han et al., 2015; Jo et al., 2019*).

Pitch is a mixture of polycyclic aromatic hydrocarbons, in which the percentage of carbon varies from pitch to pitch, depending on the origin. Petroleum pitch contains lower percentage of carbon compared to the coal tar pitch (*Sharma et al., 2020; Kershaw et al., 1993*).

The starting product of coal tar pitch is coal, and normally pitch is a by-product of the coking of coal to produce metallurgical coal coke. The production starts with the heating

of coal at T of c. 1100°C to produce coal coke, and the by-products like coke oven gases, coal tar light oil, and coal tar. The coal tar pitch is produced by distillation of the by-product coal tar (*Wombles et al., 2016*).

Pitch is also produced from petroleum and the different characteristics of petroleum pitches vary as functions of feedstocks and manufacture processes. In general, the most common process to produce petroleum pitch starts from "solvent deasphalting", which is used to separate fractions of heavy solvents.Following this stage, the "oxidation" process consists on the oxidation of heavy petroleum hydrocarbons, and the following "thermal treatment" consists in heating the product at temperatures from 300° to 480° C. The resulting product is used to produce the required petroleum pitch quality (*Wombles et al., 2016*).

2.5 Applications

Graphite is principally used in foundry and refractory industries (amorphous graphite), high quality foundry, powder metallurgy, and battery market industries (flake graphite and synthetic graphite), high-quality carbon brushes, brake lining, and lubricants (vein graphite and synthetic graphite; *Fernley 2020*, *Robinson et al., 2017*). About 25% of the worldwide graphite production is for the lithium-ion battery (LIB) sector (*Handl, 2021*), and the two types of graphite used for the LIB industry are synthetic graphite and flake graphite, which are mixed to produce the anode. The object of this thesis is the graphite sector for lithium-ion batteries for domestic electric vehicles (EVs).

2.6 What is a lithium-ion battery

Lithium-ion batteries (LIBs) have three main components: anode, cathode, and electrolyte. The anode (negative charge) is made of graphite, i.e., a mixture of flake graphite (natural) and synthetic graphite as previously explained. The cathode (positive charge) is composed of a mixture of metals (Li, Co, Ni, and Mn), what I tested in Elkem Vianode was a lithium-nickel cathode, the most used for the EV industry. The electrolyte is a solution made of ionic compound and solvent such as water, and it provides the ion transport between anode and cathode (*Fernley 2020*). In this work, I present data on the Li-Ni batteries used in the EV industry.

An important characteristic of the LIBs used for the EV industry is that they are rechargeable, thus they are able to accumulate energy and release it thanks to the ions and electrons fluxes. Graphite is an ideal anode material thanks to its high thermal and electrical conductivity, its high thermal resistance, and its layered structure. During the

charging process, the Li ions and electrons move from the cathode to the anode, the ions pass through the electrolyte in the inner part of the battery and they place between two graphite layers, while the electrons move in the outer part of the battery. This process continues until all the lithium ions are placed between the anode layers (charging process). Then, when the car is in function, the ions go back to the cathode (discharging process, Fig. 3).

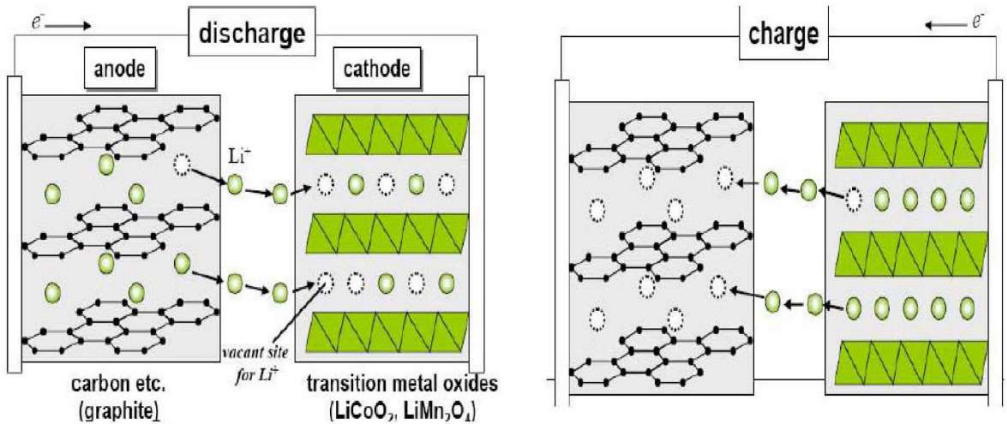

Figure 3. Charge/discharge and electrode reaction of Li-ion battery (Lee et al., 2014)

3. Methods

3.1 Approach

This master thesis has been developed between the University of Bologna, the Norwegian University of Science and Technology (NTNU) and Elkem Vianode, a company located in Kristiansand (Norway) which deals with synthetic graphite and research on graphite recycling. The first part of this work consisted in study of data on synthetic graphite production and recycling studies. This work was aimed at defining the current level of knowledge regarding composition and morphologies of green coke, synthetic graphite, graphitization residues, natural graphite, and recycled graphite (before, during, and after the recycling process). A specific objective was compiling SEM-EDS, XRD, XRF, and TEM data on these processes. The TEM analysis has been done at NTNU thanks to the partnership between Elkem and NTNU.

For the second part of the master thesis project, I spent one month at NTNU and the rest in Bologna. This part was focused on data elaboration by using the actual and experimental graphite global systems that I developed in Elkem Vianode.

3.2 Mineral Analyses

The analysed samples are seven and six of them come from big product batches, this causes possible differences in composition because of the batches' inhomogeneity. The remaining sample doesn't come from big batches but from the degassing tube into the furnaces used for the graphitization of green coke. The samples in exam are natural graphite, green coke used for the synthetic graphite production, synthetic graphite, graphitization residues deposited on furnaces degassing tube, graphite before recycling, graphite after purification, graphite after recovery. All the samples are powder, except for the graphitization residues, which have been analysed by preserving the original morphology of the material.

Table 2. Performed analyses for each sample. SEM-EDS (Scanning Electron Microscope and Energy Dispersive X-ray Spectroscopy), XRD (X-ray Diffraction Analysis), XRF (X-ray Fluorescence), TEM (Transmission Electron Microscopy).

	SEM-EDS	XRD	XRF	TEM
Natural graphite	x	x	x	x
Green coke	x		x	
Synthetic graphite	x	x	x	x
Graphitization residues	x			
Graphite before recovery	x	x	x	
Graphite after purification	x	x	x	
Graphite after recovery	x	x	x	x

The objectives of the mineral analysis are to observe the composition and structural evolution of the synthetic and recycled graphite productions, the first one by analysing green coke and synthetic graphite, while the second one by analysing graphite before recovery, graphite after purification and graphite after recovery samples. Another objective is to evaluate what are the main losses during the graphitization process of the synthetic graphite production, and this is possible also thanks to the graphitization residues analysis. Instead, the natural graphite analysis has the objective of comparing its compositional and structural features with the ones of graphite after recovery. The analytical methods performed are SEM-EDS, XRD, XRF, and TEM (*Table 2*).

3.2.1 Scanning Electron Microscopy (SEM) and Energy Dispersive X-ray Spectroscopy (EDS)

The Scanning Electron Microscope (SEM) provides high resolution images (1nm) of a sample. While the SEM is used to analyse the morphological aspect of a sample, the EDS detector (Energy Dispersive X-Ray Spectroscopy), which is incorporated to the SEM machine, provides a qualitative and a quantitative chemical composition of a selected point. The SEM machine used in Elkem was a Merlin Compact of Zeiss with a Schottky FEG (Field Emission Gun) emission, and DENKA TFE ZrO/W electron beam source. The entire SEM chamber had an ultra-high vacuum chamber between 10^{-7} and 10^{-8} Pa.

The used EDS detector was a Silicon Drift Detector (SDD) XFlash® 6 | 30, from Bruker.

The SEM analysis detects electrons generated by the interaction between the electron beam and the sample, the secondary (1-10 eV) and backscattered (>50eV) electrons in order understand the morphology of the sample in exam, while the EDS detects the X-ray emissions to know the chemical composition of a selected point. Sample preparation wasn't necessary because the samples were all conductive.

3.2.2 XRD – X-ray diffraction analysis

The X-ray diffraction is a qualitative and semi-quantitative analysis, which is used to identify the crystalline phases of a sample by the determination of its atomic and molecular structure thanks to the interaction between the X-ray beam and the powdered sample.

Before analysis, the green coke and the graphite before recycling samples were crushed and milled because of their coarse particles. Then, the five samples were shipped to the XRD lab in Elkem Vianode in which the operator has inserted the samples in a 25 mm back-loading sample holder.

The analyses were performed with the diffractometer Bruker D8 Advance with a Cu source at 40 kV and 40 mA with a Ni filter, the 2θ was from 10° to 90° with a step size of 0.02° and a time per step of 1s. The goniometer radius was 217.5 mm, and the used detector was the LynxEye Position Sensitive.

After analysis, which can take up to 1 hour, the intensity of the X-ray diffraction pattern of the sample is plotted as a function of 2θ.

3.2.3 XRF – X-ray fluorescence

The X-ray fluorescence technique is a quantitative (until few ppm) and qualitative analysis technique used for the elemental analysis of liquid and solid samples. This method is based on the characteristic X-rays release from the atoms' ionization.

The XRF used in Elkem Vianode is the Malvern Panalytical wavelength dispersive XRF (WD-XRF), the X-ray source was a rhodium tube of 4kW, and the detector was 48-position automatic sample changer. The data were processed with the software SuperQ6.

The advantages of XRF are that the analysis is not destructive, and it gives the possibility to analyse of different elements in a short time, while the disadvantage is that it is possible to detect only the elements with between Na and U, gaseous elements excluded.

3.2.4 TEM – Transmission Electron Microscopy

The Transmission Electron Microscopy is useful to gather structural information of a solid via transmission of an electron beam through the sample. and for this the samples for the TEM analysis must be 100nm of thickness. In the case of graphite, the graphite samples are composed by round particles, and thus, it is necessary to cut one single particle before the TEM analysis. The preparation of the TEM samples was performed with a Helios G4 UX dual-beam focused ion beam (FIB) from FEI/Thermo Fisher. Before cutting the region of interest, it was necessary to deposit layers in order to protect the sample below. The first part of the protection coating was deposited by electron beam assisted deposition to avoid any ion-beam damage into the region of interest. The second part of the protection coating, which is the thickest, was deposited by Ga^+ ion-beam assisted deposition. Then, the coated samples were cut with the focused ion beam (FIB) at 30kV acceleration voltage for the coarse thinning, while the final and more accurate thinning was done at 5kV on each side of the lamella to minimize the ion-beam damages, then the samples were transferred to the Cu half grids with a Tungsten tip.

The TEM analyses were performed with a double spherical aberration corrected, cold field emission gun (FEG) "JEOL ARM 200FC" TEM model, operated at 200kV. TEM imaging is performed thanks to a parallel electron beam on the sample focused by three condensers. The electrons elastically scattered are detected by a bright field detector, thus the unscattered (transmitted) electron beam, which pass through the sample between one atom and another, are detected as white areas, while the electron beam who hits the atoms of the sample is elastically scattered and thus the atomic positions appear dark.

3.3 Material Flow Analysis

3.3.1 System definition

Material Flow Analysis (MFA) is an analytical method that quantifies and evaluates/investigates the material flow and stocks of an anthropogenic and geogenic system, which are defined in space and time (*Brunner et al., 2004*).

The system I defined focused on the graphite flow for the anodes of passenger EVs' LIBs and it is the result of my understanding and studies during the internship in Elkem Vianode. In addition, I had some help even from Skaland Graphite AS, a company engaged in the production of high-quality flake graphite, in order to have some additional information on natural graphite production.

In MFA, the system definition considers all the stages of production that involve movements of stocks and their efficiency. In this study, the data about the efficiency of each process of synthetic graphite production, as well as the details of the process of graphite recycling, are confidential data. Hence, in the definition of the generic system given below (Fig. 4), I only insert the generic process information and efficiencies.

The synthetic system definition of the graphite flow for Li-ion batteries uses four different colours to represent four pathways of the system, namely synthetic graphite production (yellow), natural graphite purification (red), LIB and EV production, use and dismantling (blue), and graphite recycling (green). In the following paragraphs, these pathways of the system will be explained.

Synthetic graphite production. The detailed system is shown in Figure 5. After crushing and drying (*raw material handling, Fig. 5* - process 1), the green coke is submitted to the *impact milling* process (flow A1-2), which has the scope to reduce the size of the green coke pieces (process 2). After the impact milling, the green coke particles must be shaped as round as possible, and this process is called *shape milling* (process 3), the accepted grain size after this process is between 16 and 20µm (flow A3-4). Then, the green coke is mixed with the pitch (flow A0-4) and agglomerated (*agglomeration process,* process 4). Subsequently, the material is ready for the *graphitization* process (process 5), which consists of an exposure to extremely high T of the green coke agglomerated with pitch. This heating must be slow in order to simulate the natural condition of crystallization. To be specific, the furnace heats up the material with a constant T, and then, the maximum temperature is maintained constant for several hours in order to reach the highest degree

of graphitization. During this holding period, the C atoms inside of the material are rearranged into a more ordered structure, the graphite atomic structure.

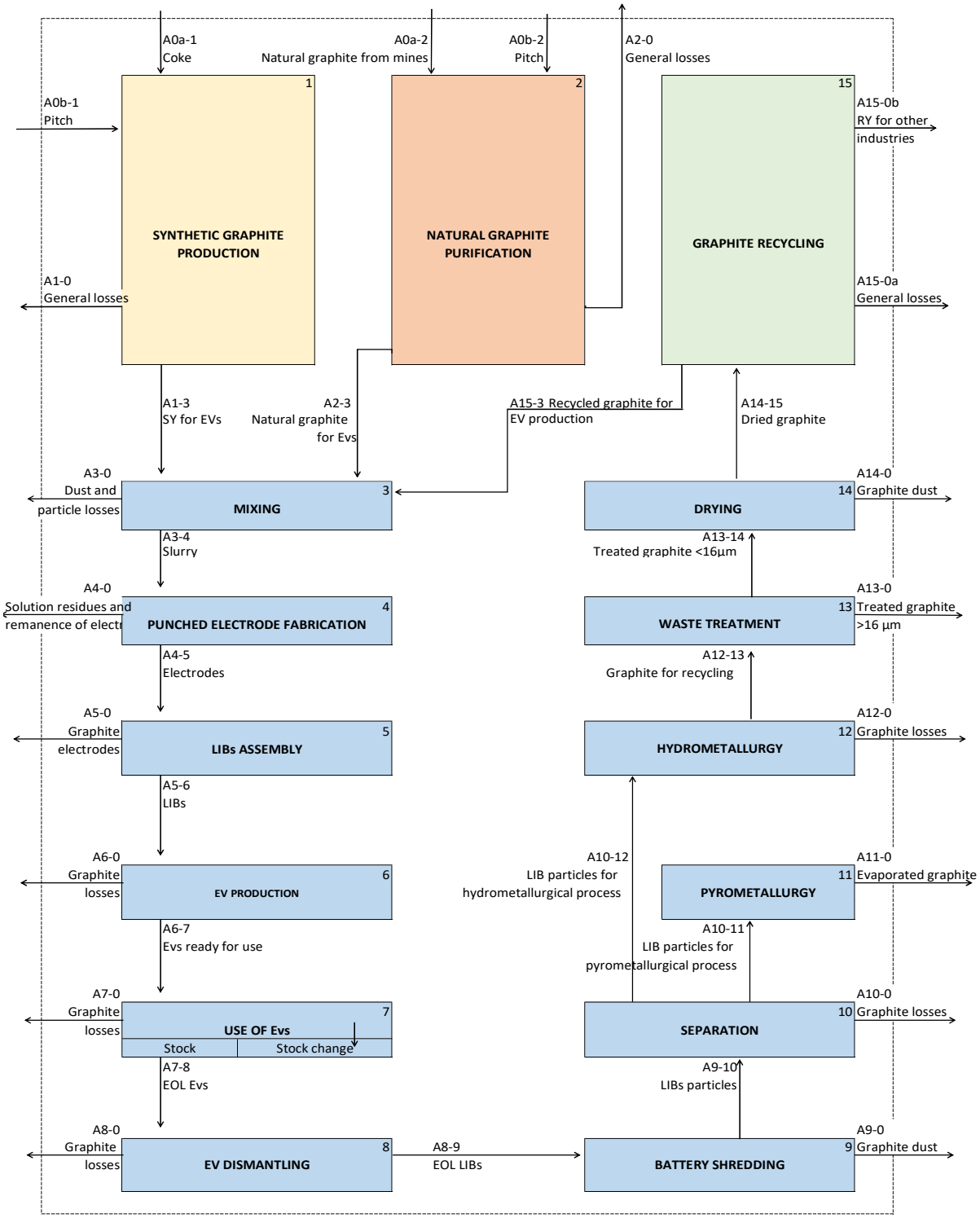

Figure 4. Graphite flow system for electric vehicles' Li-ion batteries. Arrows: material flows, boxes: processes, dashed box: system boundary. Yellow box: synthetic graphite production, red box: natural graphite purification, green box: graphite recycling, blue boxes: LIB and EV production and dismantling.

During the crystallization process, the trace elements of the green coke (impurities) like Ti, Ca, V, Co, Ni, S, W, and even a little fraction of carbon, evaporate. When the holding period ends, the cooling process can start. After graphitization, the material, which is now synthetic

graphite (SY, flow A5-6 of Fig. 5), must be coated with other pitch (flow A0-6). This process (*Finish coating,* process 6) adds other carbon material to the surface of the graphite particles, and this makes them less porous and more conductive. The finish coating is followed by *carbonization* (process 7), which consolidates the previous coating.

On a later stage, the synthetic graphite particles are sieved (*sieving,* process 8) and the grains with a diameter smaller than 45μm are accepted (flow A8-9), while the other are considered waste (flow A8-0). The next step is the *magnetic separation* (process 9), which is a process that checks if there are any ferromagnetic minerals. If present, these minerals are trapped with magnets and wasted (flow A9-0). The system ends with the last step which is the *synthetic graphite product handling* (process 10)*,* which consists of preparing boxes for the anode fabrication companies.

The efficiency of the entire synthetic graphite production system was evaluated at about 65%.

Natural graphite purification. The detailed system is shown in Figure 6. The process leading to the purification of natural graphite is the same as that of the synthetic graphite production system. A fundamental difference is the absence of the graphitization process because the treated material is already graphite; thus, the material doesn't need significant heating like in the graphitization (crystallization). This entire process has a total average efficiency of 50%, from the mining process to the final product.

Dismantling. Industry data show that the global average of graphite used for the LIBs production is a mixture of 50% synthetic graphite and 50% natural graphite. As a result, the first production step is the *mixing* (process 3, Fig. 4, efficiency c. 95%), in which the two types of graphite are mixed with CMC (Carboxymethyl Cellulose) binder, JSR © binder, and carbon black (carbon content >97%). After this stage, the solution is cast on a Cu foil and dried at 85°C for 1 or 2 hours. Successively, the electrode foil is ready for the punching (*punched electrode fabrication,* process 4, Fig. 4, efficiency 95%). In this process, a punching machine creates several round electrodes with a diameter of about 12

mm, even if this parameter depends on the dimensions of the final product. The electrodes are punched, and they are kept in a vacuum at 130°C for 16h. Then, the electrodes are used for the *LIBs assembly* (process 5, Fig. 4, efficiency 100%, no graphite losses), which must be made in a water and oxygen-free environment. The process starts with the cleaning of the Li-chips from the oxide layer with an electric brush. Then, it is necessary to put 50µl of electrolyte by using a pipette at the base of the cell case and then to put the graphite anode with the graphite side facing up. Successively, it must be placed other 50µl of electrolyte above the graphite anode and after that a separator, which separates another 50µl of electrolyte and the brushed Li-chips. The last steps consist in put the Ni foam on the Li-chips, and the spacer on the Ni foam. To conclude the LIBs assembly process, it is necessary to put the spring and make sure that all the components are placed in the centre of the coin cell, then the cell case to close everything can be added. From the bottom to the top, the coin cell has the following configuration: cell case, anode, separator, Li-metal, Ni foam, spacer, spring, cell case cap. Then, the LIBs are assembled to the EV (*EV production,* process 6, Fig. 4, efficiency 100%, no graphite losses), and EVs are ready for use.

The dismantling starts after the end of life (EOL) of the EVs (flow A7-8), but this last flow is variable depending on the year. Current work (Aguilar Lopez, unpublished data, Table 3), show that the rate of produced vehicles (flow A6-7) and EOL vehicles up to the year 2050. During the use of EVs (process 7) there is no graphite losses, and thus the efficiency of this process is 100% (assumption). At the EOL, the vehicles are dismantled (*EV dismantling*, process 8, efficiency 100%) and the EOL LIBs (flow A8-9) go to the *battery shredding* (process 9, efficiency 95%). Then, a separation is carried out between the different components of the battery (*separation*, process 10) and the non-recyclable parts of the LIB are send (flow 10-11) to the pyrometallurgical process (11). There, 100% of graphite is lost. Actually, this last process is used even for graphite components of the EOL LIBs, including graphite, which is not recycled today. Despite this, it is possible to observe that in the system (Fig. 4) there is also another option in order to make the scenario previsions: the graphite recovery for the recycling process.

Graphite recovery can be performed thanks to the hydrometallurgical (process 12) treatment of the EOL LIBs instead of the pyrometallurgical one. The hydrometallurgical process consists on the separation of graphite from the other EOL LIBs by floatation and it has an efficiency of 93% (*Yang et al., 2021*). After the hydrometallurgical process, the material is selected and sieved (*waste treatment,* process 13, efficiency 95%), the accepted

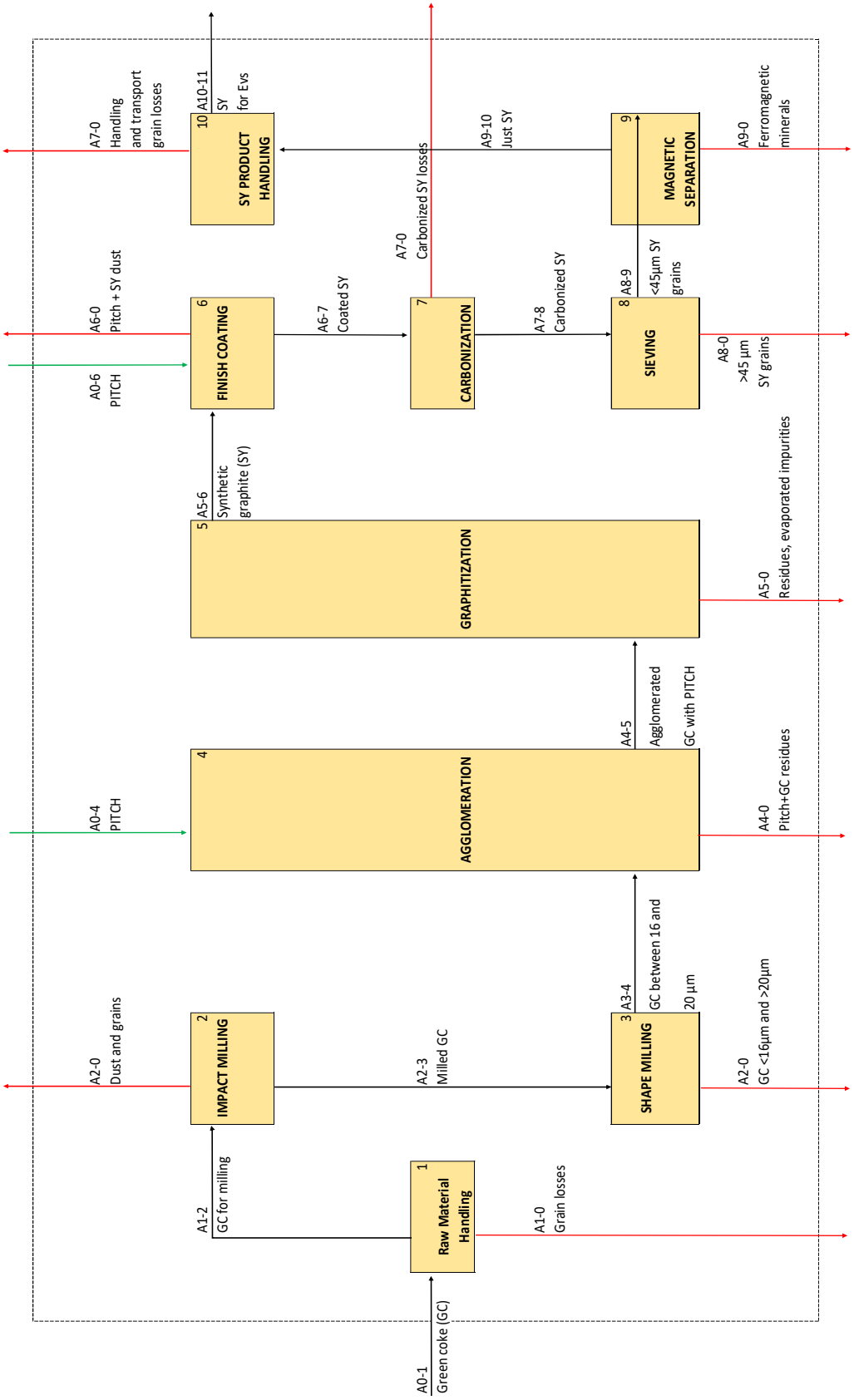

Figure 5. Details of synthetic graphite production. Arrows: material flow, boxes: processes.

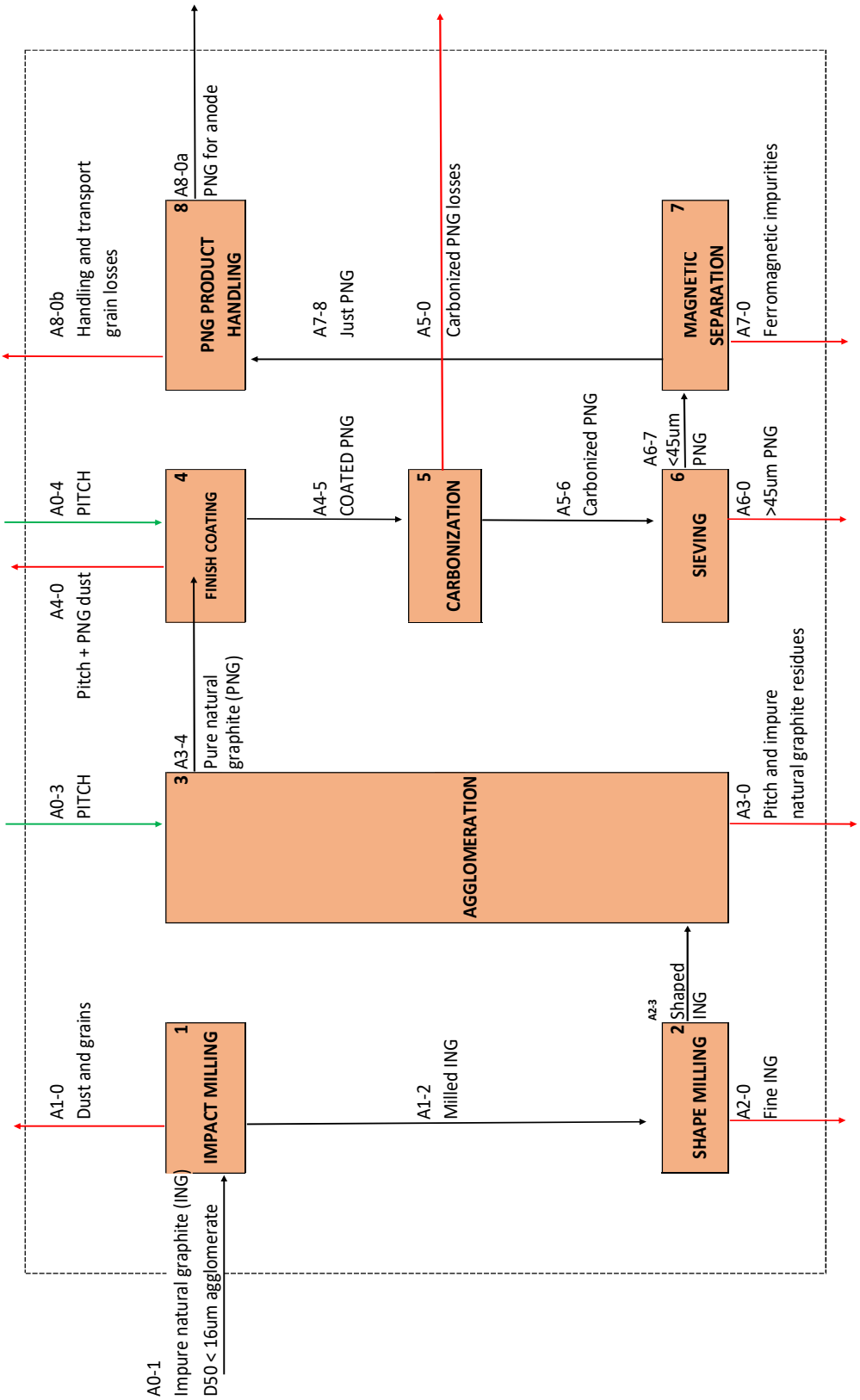

Figure 6. Detailed system of natural graphite purification. Arrows: material flows, boxes: processes

material for the recycling process has a grain size <16µmand the rest is waste (flows A13-14 and A13-0). Then, the sieved material must be dried from the water of the hydrometallurgical water (*drying,* process 14). The efficiency of the drying process is 100% because there are just losses of water and not graphite.

Graphite recycling. The detailed system is shown in Fig 7. The recycling process of graphite from old LIBs can start when the recovered graphite has a C content above 95%. Then, the material is transported and crushed (*material handling*, process 1, Fig.7) and subsequently it is treated (*pre-processing,* process 2, Fig. 7) to adjust and deagglomerate particles (remove moisture, organic components, binders). After this, the treated graphite goes to the *thermal purification* (process 3, Fig. 7) which has the purpose to remove impurities, remaining sulphur, lithium, and fluorides. The purified graphite goes to the *surface treatment* (process 4, Fig. 7) in which graphite can be coated and thus the conductivity is improved. The last process is the *recycled product handling* (5) and, in this process, the recycled graphite is sieved, tested, and packed.

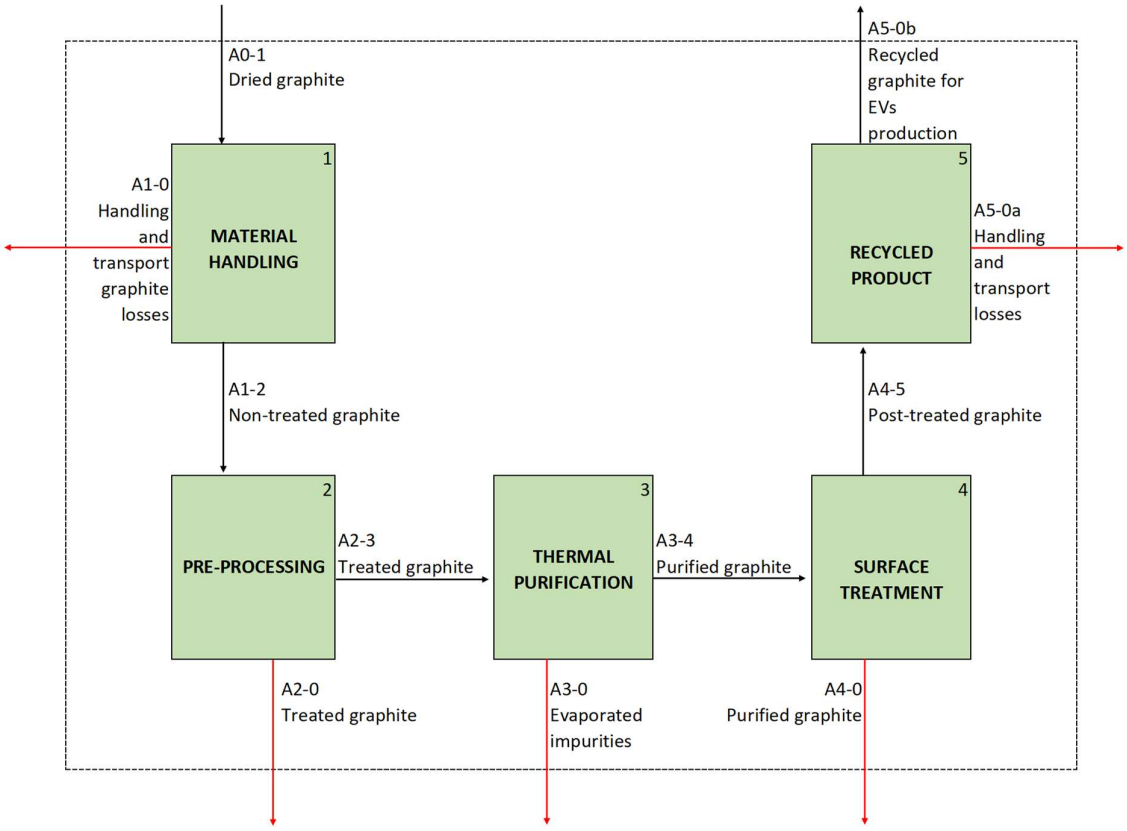

Figure 7. Detailed recycling process of graphite from LIBs.

The total efficiency of the graphite recycling system is 90%. In this work I suppose that recycled graphite takes the place of the natural one, thus, scenarios studies were carried out take into consideration that the anode production is made with a mix between synthetic and recycled graphite. The percentages are still an object of study; therefore, all of the percentage experimented in the scenarios are assumptions.

3.3.2 Dynamic Material Flow Analysis and scenario analysis

The dynamic Material Flow Analysis is used to simulate the dynamic behaviour of the system in a within a specific time frame. For this project, the period is between 2022 and 2050, and the dynamic analysis is used to quantify 3 different scenarios, which include the recycling option, based on changes of the variables that are the input and output of produced cars and EOL cars. In these three scenarios, natural graphite is not included, but replaced by the recycled one, which is mixed with the synthetic one during the anode production. In addition, the "current graphite flow" for EV lithium-ion batteries is quantified in order to have a picture of the situation in 2021 and even the graphite flow from 2021 up to 2050 without considering any recycling option in order to have a "baseline scenario".

With regards to the battery size, it is assumed that on average, each passenger electric vehicle contains 70 kg of graphite and I also assume that the battery size doesn't change with the variation of graphite mixture.

Table 3, was used to quantify the "current graphite flow" for the year 2021, the "baseline scenario" from 2022 to 2050, and even the three different scenarios for the future years.

The process involving input and output modifications is number 7 (*Use of EVs*, Fig. 4), the flows are A6-7 and A7-8 (Fig. 4). The given data are named Input_year, which are the number of sold cars but in decimals, thus, the data in the table must be converted into integer:

$$Input\_year \cdot 10^6 = EV\_inflow$$
$$Output\_year \cdot 10^6 = EV\_outflow$$

Equation 1

Then, the number of vehicles (EV_Inflow) must be multiplied by 70 kg (Graph_EV, see Appendix), which is the graphite present, on average, inside a passenger electric vehicle, this data must be converted into kt:

$$EV\_inflow \cdot Graph\_EV \cdot 10^{-6} = A6 - 7$$

$$EV\_outflow \cdot Graph\_EV \cdot 10^{-6} = A7 - 8$$

Equation 2

The rest of the flow equations and given data can be found in the Appendix.

Table 3. Produced and sold EVs (input), EOL EVs (output), and EV still in circulation (stock), from 2022 to 2050. (Aguilar Lopez, unpubl data.)

Year	Stock	Inflow	Outflow	Unit
2021	29.116124	6.641523	0.751142	Million
2022	36.328041	8.166948	0.955031	Million
2023	45.115335	9.997045	1.209750	Million
2024	55.765556	12.176461	1.526240	Million
2025	68.593500	14.745198	1.917254	Million
2026	83.928394	17.732384	2.397490	Million
2027	102.097040	21.152340	2.983695	Million
2028	123.403136	25.000791	3.694695	Million
2029	148.099267	29.247415	4.551284	Million
2030	176.357817	33.834518	5.575968	Million
2031	208.244885	38.679584	6.792516	Million
2032	243.699879	43.680244	8.225249	Million
2033	282.525735	48.723921	9.898065	Million
2034	324.390892	53.698321	11.833164	Million
2035	368.844288	58.502915	14.049518	Million
2036	415.338914	63.055753	16.561127	Million
2037	463.260522	67.296801	19.375193	Million
2038	511.957334	71.187197	22.490385	Million
2039	560.771104	74.709192	25.895422	Million
2040	609.063894	77.860940	29.568151	Million
2041	656.242032	80.653497	33.475358	Million
2042	701.775915	83.107297	37.573414	Million
2043	745.215802	85.249699	41.809812	Million
2044	786.201793	87.111495	46.125503	Million
2045	824.469514	88.725603	50.457882	Million
2046	859.850614	90.125201	54.744101	Million
2047	892.267773	91.341562	58.924403	Million
2048	921.725209	92.402554	62.945119	Million
2049	948.297650	93.333504	66.761063	Million
2050	972.116740	94.156201	70.337111	Million

The purpose of the so-called scenario study is to understand what the best approach to the graphite recycling for the future years could be, and even evaluate if recycling is replaceable with natural graphite; thus, how the synthetic graphite request changes as a function of the recycled one. In order to perform the scenario studies, the flows A10-11, A10-12, A15-3, A15-0b, which represent respectively “Graphite LIB particles for

pyrometallurgical process", "Graphite LIB particles for hydrometallurgical process", "Recycled graphite for EV production", "Recycled graphite for other industries" (Table 4) have been changed for each scenario in terms of percentages of graphite mass which pass in through these flows. The data and context used for each scenario are resumed in Table 5.

Table 4. Variables (flows) parameters changed for each scenario.

Flow Parameter	Name
A10-11	Graphite LIB particles for pyrometallurgical process
A10-12	Graphite LIB particles for hydrometallurgical process
A15-3	Recycled graphite for EV production
A15-0b	RY for other industries

Table 5. Parameters used for each scenario.

Scenario	Name	Year	Parameter	Parameter	Parameter	Parameter
A	Baseline scenario	2021, up to 2050	100%	0%	0%	0%
B	100% recycled and used	2022, up to 2050	0%	100%	100%	0%
C	100% recycled, gradual use for LIBs	2022	0%	100%	5%	95%
		2032	0%	100%	10%	90%
		2042	0%	100%	15%	85%
		2050	0%	100%	20%	80%
D	Gradual recycling, 100% for LIBs	2022	75%	25%	100%	0%
		2032	50%	50%	100%	0%
		2042	25%	75%	100%	0%
		2050	0%	100%	100%	0%

3.3.2.1 Current graphite flow and baseline Scenario

The first scenario doesn't include any kind of graphite recycling and it shows what will be the synthetic graphite and natural graphite demands if the LIBs for EVs between 2021 and 2050 are not made with recycled graphite. This is a "business as usual" scenario, which has been developed because of its possible interesting results on synthetic and natural graphite variations. The "baseline scenario" is thus compared against the other three in order to evaluate the two opposite ways of the EOL electric vehicles dismantling.

3.3.2.2 "100% recycled and used" scenario (B)

The second scenario is based on the possibility that all the graphite from LIBs of EVs is recovered, sent to the graphite recycling process, and used for the LIBs for EVs industry instead of natural graphite. The scenario is presented up to 2050, considers the recycling process of Fig. 7, and it is made using the data of Table 3, which are used in combination with equations 1 and 2. With regard to the pyrometallurgical process (process 11, Fig. 4), all of the graphite is recycled in this scenario, and thus 100% of it goes (flow A10-12) for the hydrometallurgical process (process 12). This scenario is useful to evaluate what the

maximum level of recycled graphite for EVs' LIBs production up to 2050 is. For this, the amount of synthetic graphite is rearranged based on the amount of produced recycled graphite for EVs' LIBs.

3.3.2.3 "100% recycled, gradual use for LIBs" scenario (C)

This scenario includes the recycling process, and it shows what could be the contribution of the recycled graphite if all the EVs' LIB are recycled but not all the recycled graphite is re-used for the LIB production. So, the scenario, which is made thanks to table 3 by changing input and output flows (flows A6-7 and A7-8, Fig. 4) of "Use of EVs" process (process 7, Fig. 4) as equations 1 and 2 explain, shows that the 100% of the graphite from LIBs goes for the hydrometallurgical process, and thus for the recycling one, but not all the recycled graphite is for EVs' LIBs: just the 5% in 2022, 10% in 2032, 15% in 2042, and 20% in 2050 of the graphite necessity is covered by the recycled one while the graphite lack is replaced by additional synthetic graphite. The remaining recycled graphite goes for other industries like foundry, powder metallurgy, high-quality carbon brushes, lubricants, or even for other E-devices market (flow A15-0b, Fig. 4).

This scenario is based on the fact that it is possible that the efficiency of the world recycled graphite couldn't be at the best as the synthetic and natural ones. For this, the increasing percentages of recycled graphite for EVs' LIBs reflect its possible demand for the EVs for the next years, which will increase thanks to the efficiency improvement of the recycled material.

3.3.2.4 "Gradual recycling, 100% for LIBs" scenario (D)

The fourth and last scenario includes the recycling process (Fig.7) and it is based on the fact that it is unlikely that all of the graphite from LIBs of EVs of the entire world will be recovered through the hydrometallurgical process. This scenario starts with a 25% of graphite for the hydrometallurgical process in 2022, 50% in 2032, 75% in 2042, and 100% in 2050, while the remaining percentages represents the graphite that is lost by the pyrometallurgical process. The forecasts were made thanks to Table 3 by the substitution of the input and output flows (flows A6-7 and A7-8) of the process "Use of EVs" (process 7, Fig. 4), as equations 1 and 2 explain. Even this scenario doesn't take into consideration the use of natural graphite in the system.

3.3.3 Limitations and Uncertainties

The results arising from the scenario analysis have some limitations given by the uncertainty of the data. First, the efficiency of the natural graphite purification process depends on the company and on the studied country. In this case I applied data from Skaland AS, which provided the global average. As regards the synthetic graphite production efficiency, the value used in this represents the one of Elkem AS but the global average could be different. The same thing happens for the recycled graphite production. The efficiency data for this process is based on an experimental process of Elkem, which is not industrially used today. In addition, the procedures for LIB and EV construction, and LIB and EV dismantling (the blue part of the system), are composed by processes for which no clear and realistic efficiency data were found. I thus made different assumptions based on knowledge gathered during the internship in Elkem Vianode.

4 Results

4.1 Mineral analyses

4.1.1 SEM-EDS

4.1.1.1 Natural Graphite

From the SEM images, the natural graphite powder comes with a characteristic potato shape. The surface of the particles is smooth with visible flat layers. There are no shape edges, and the whole the sample grain size is quite homogeneous, between 10 to 15 µm (Fig. 8).

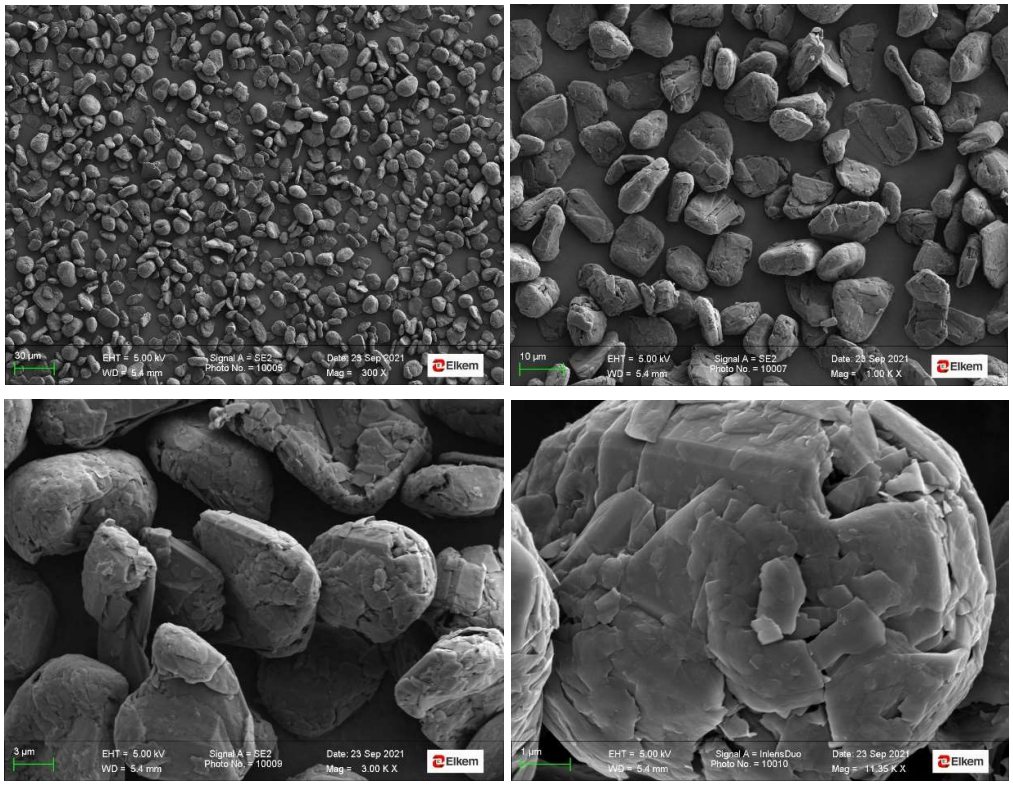

Figure 8. Natural graphite SEM analysis

From the EDS (Table 6) analyses we can observe that the whitest parts of the sample have poor carbon composition. The spectrum no. 59 is mainly composed by N and Ti, while spectrum 67, in addition to Ti and N, also has C. There are even spectra 62 and 65 with a composition of C, O and Zr.

The other spectra are not located in the whitish area, but on the grey particles which represent most of the sample. As spectra 61, 63, 64, 66 and 68 show, the composition that they show is mainly made of carbon, with percentages between 99.51 and 100.

Table 6. Results of EDS analyses of Natural Graphite sample.

Atomic concentration [%]										
Spectrum	C	N	O	Mg	Al	Si	Ti	V	Nb	Zr
59		52.88		0.3	0.44	0.28	44.59	1.03	0.47	
60			100							
61	99.51		0.49							
62	57.86		29.12			0.87				12.15
63	100									
64	99.8		0.2							
65	66.27		17.42							16.31
66	99.76		0.24							
67	35.86	39.15		0.3	0.14	0.17	24.4			
68	99.85		0.15							

4.1.1.2 Green coke

Petroleum green coke images from the SEM analyses (Fig. 9) show that the particles are angular, and the grain size is not homogeneous. Some particles have a diameter >30µm but can reach even 100 µm although most of them have a size <20 µm. Magnifications of 1.0K X and 3.0K X show some little and whitest particles around the largest ones.

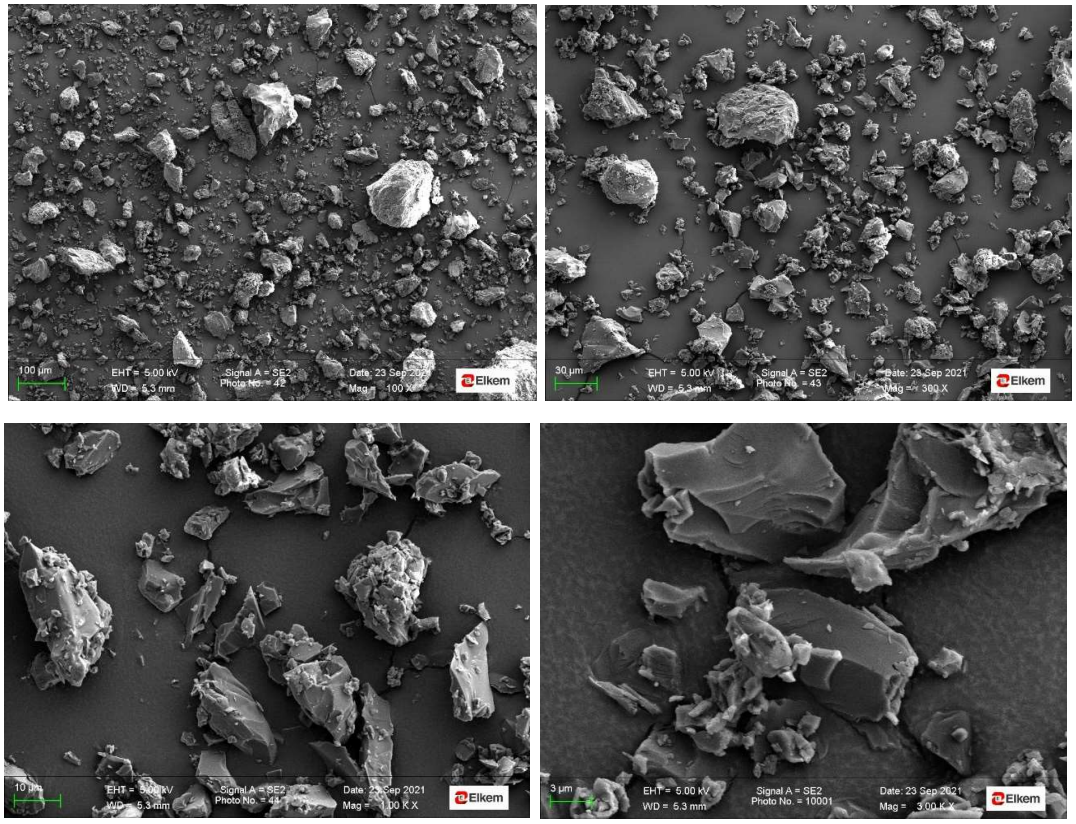

Figure 9. Green Coke SEM analysis

The EDS (Fig. 10 Table 7) analyses was made in 13 points, and we can observe that in general, the carbon percentage is relatively high in spectra 48, 49, 51, 52, 54, 57, 58 in a range between 95.05 and 96.38 %.

In any case, there are even some spectra, which are the result of the analysis on the whitest part of the sample (47, 50, 53, and 56). These analyses show that the analysed particles have a Ca component. In addition, the spectrum 55 shows a composition of just oxygen and sulphur.

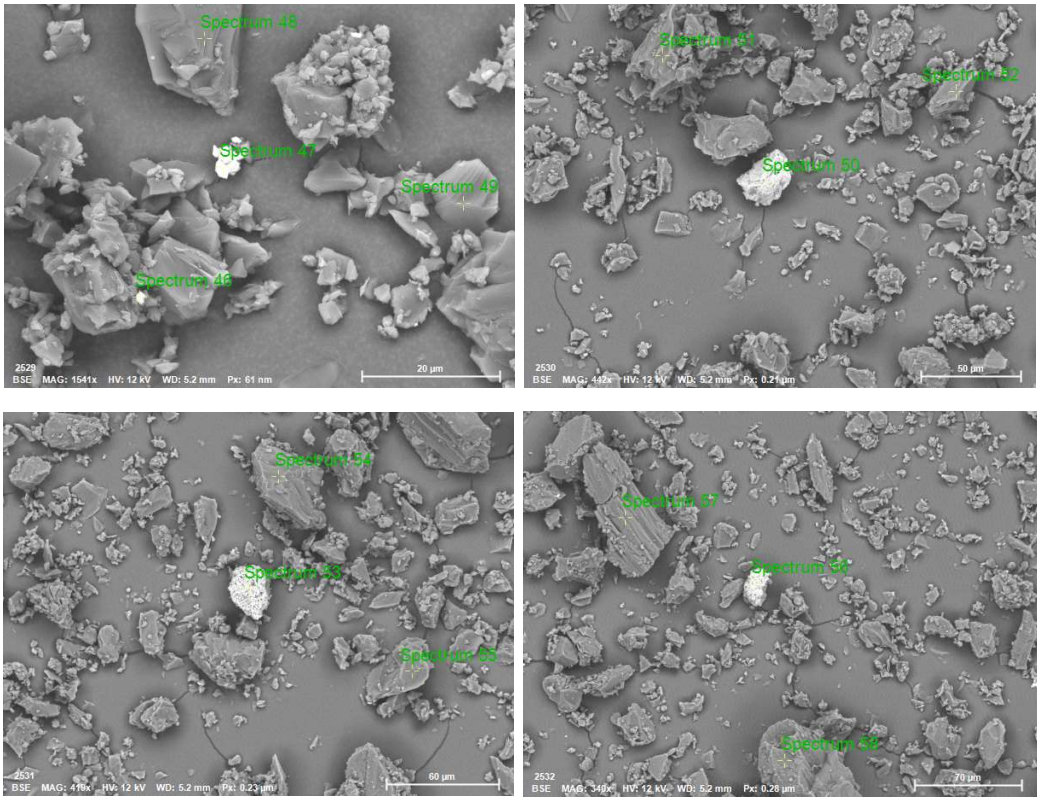

Figure 10. Backscattered electrons SEM images of Green Coke sample with the selected points (noted in green) for the EDS analysis

Table 7. EDS analysis of the Green Coke sample. Atomic concentrations in percentage of the analysed points showed in Figure 10, from spectrum 46 to 58.

Atomic concentration [%]							
Spectrum	**C**	**S**	**O**	**Mg**	**Ca**	**Si**	**Fe**
46	68.99	0.19	23.1	0.08	7.64		
47	24.02	0.38	58.89		0.79	2.57	13.35
48	96.13		3.87				
49	95.95	0.13	3.93				
50	26.21		45.97		27.82		
51	96.38	0.17	3.45				
52	95.05	0.08	4.87				
53	33.17	0.26	51.81	0.1	14.65		
54	95.33	0.1	4.58				
55		16.96	83.04				
56	10.33	0.41	65.73	0.11	23.43		
57	96.49	0.14	3.37				
58	95.6	0.1	4.3				

4.1.1.3 Synthetic graphite

The SEM images of the synthetic graphite sample (Fig. 11) shows that the particles have angular shapes, except for some cases, well show in the image at 400X of magnification, in which the shape is perfectly round or sub-round. In general, it's evident that the particles are composed by crystals aggregate, and thus, the lamellae are evident, especially in the figure at 1.00 KX of magnification. The grain size is quasi-homogeneous between 20 and 30 µm, but at the same time there even are some particles between 3 and 10 µm, and some particles with a diameter of 40 µm.

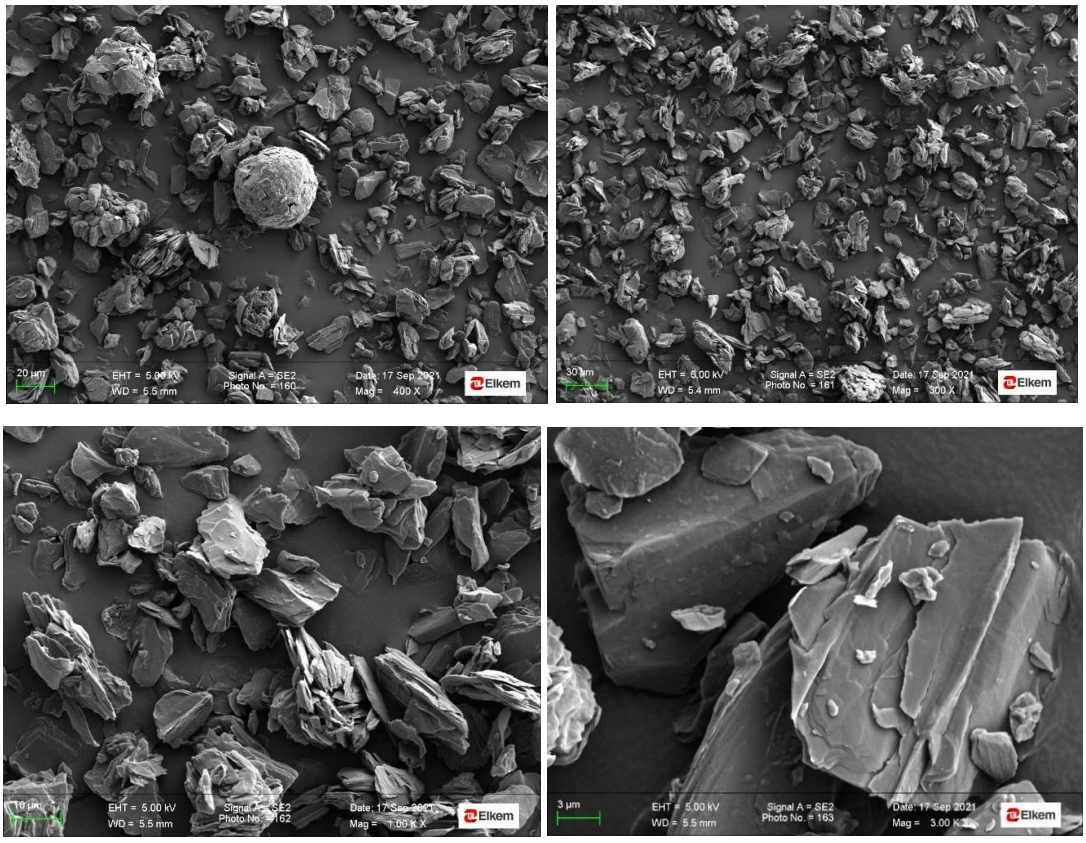

Figure 11. Synthetic Graphite SEM analysis

From the EDS analyses (Fig. 12, Table 8) of the Synthetic Graphite sample, it is possible to observe that all the selected points have a percentage of C content >98.5%. The spectra 1 and 2 are 100% pure in carbon content, while spectra 3, 5, and 6 have a percentage >99%, then, spectrum 4 has a percentage of carbon content of 98.55%.

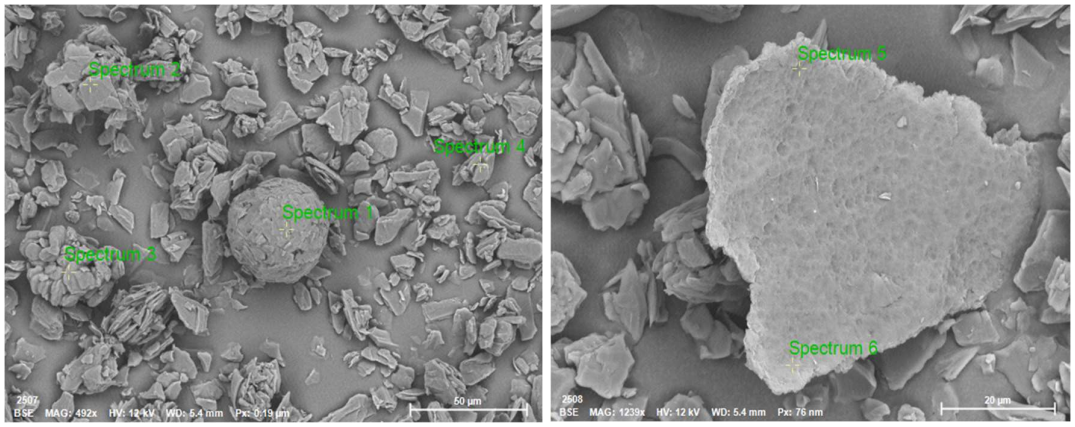

Figure 12. Backscattered electrons SEM images of Synthetic Graphite sample with the selected points (noted in green) for the EDS analysis

Table 8. EDS analysis of the Synthetic Graphite sample. Atomic concentrations in percentage of the analysed points showed in Figure 12, from spectrum 1 to 6.

Atomic concentration [%]		
Spectrum	**C**	**O**
1	100	
2	100	
3	99.58	0.42
4	98.55	1.45
5	99.02	0.98
6	99.1	0.9

4.1.1.4 Graphitization residues

Graphitization Residues samples are the residues of the graphitization process, which consists of heating up the milled Green Coke. During the graphitization process, while the carbon material crystallizes, all the Green Coke impurities evaporate and deposit along the furnace's tubes. The SEM images (Fig. 13) show three types of residues morphologies. The first one is observable in the panels a and b of Figure 13, in which the residues have round-crust structure. In panel a, the crusts are best developed with a semi-ramification, while in panel b, they are more isolated and not linked together. Fig. 13c shows a different residue morphology. In this case, residues form cauliflower shape with some little hole at some dome endings. Instead, panel 13d shows fine grained and micro-lamellar shapes.

a. 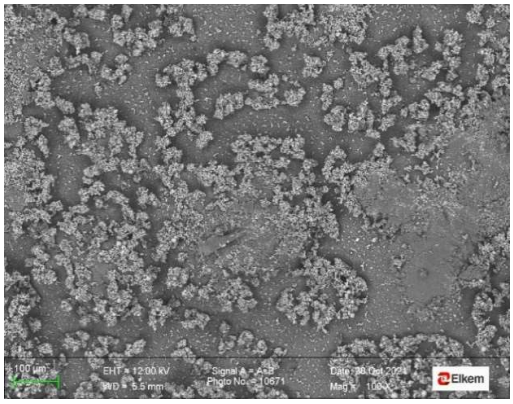

b. 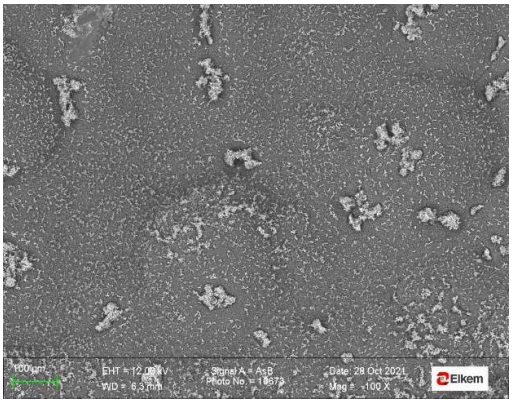

c. 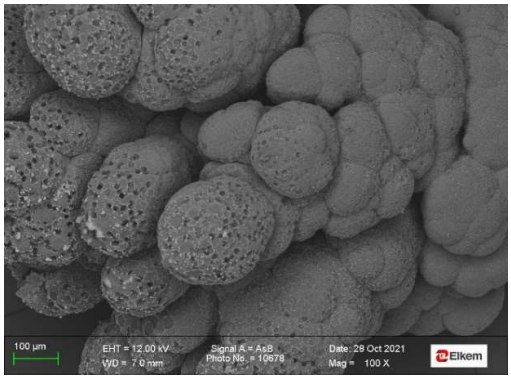

d. 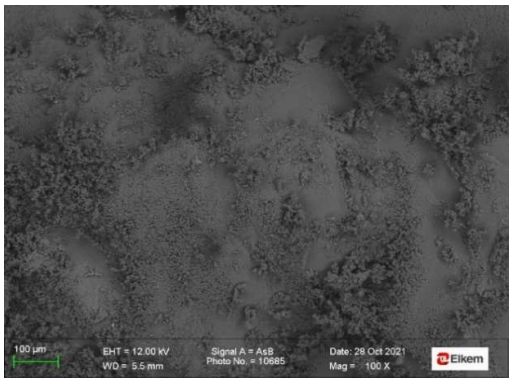

Figure 13. Graphitization Residues SEM analysis

The EDS analysis shows the chemical composition of selected points of each morphology. The round-crust shape EDS analyses (Fig. 14 and Table 9) shows a high carbon content in spectrum 1 located in the darkest zone. The other spectra 2-5, show the highest concentrations in O (>56.15%) and Ti (>22.07%), with some Ca (1.12%) in spectrum 2, vanadium (0.44<V<0.63%) in spectra 2, 4, and 5, Co (0.3%) in spectrum 3, and Ni (1.29%) in spectrum 3.

Table 9. EDS analyses of the Graphitization Residues sample. Atomic concentrations in percentage of the analysed points in Figure 14, from spectrum 1 to 5.

Atomic concentration [%]								
Spectrum	C	O	S	Ca	Ti	V	Co	Ni
1	96.19	3.49	0.1	0.1	0.11			
2		56.15		1.12	42.12	0.6		
3		69.54			28.87		0.3	1.29
4		77.3			22.07	0.63		
5		75.9			23.66	0.44		

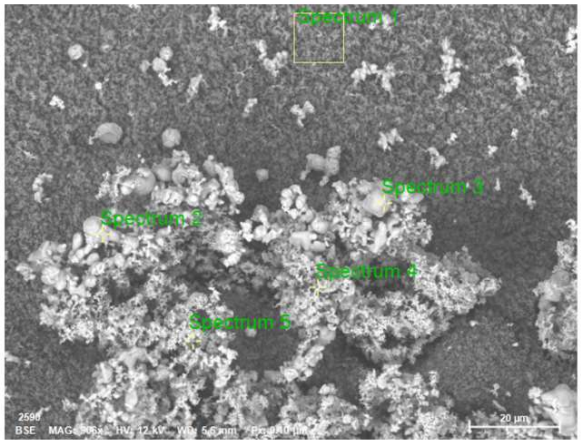

Figure 14. Backscattered electrons SEM images of Graphitization Residues sample with the selected points (noted in green) for the EDS analysis and

The EDS analyses of the residues with a cauliflower shape (Fig. 15 and Table 10) show that the chemical composition has a higher carbon content. The first two spectra, 1 and 2, have more than 99.28% of carbon content. Spectrum 3, which has a whitest colour, has a composition made of 70.17% of carbon, and 19.44% of oxygen. In addition, spectrum 3 contains even calcium (6.49%), tungsten (2.65%), nickel (0.35%), and sulphur (0.89%).

Table 10. EDS analysis of the Graphitization Residues sample. Atomic concentrations in percentage of the analysed points showed in Figure 15, from spectrum 1 to 3.

Atomic concentration [%]						
Spectrum	C	O	S	Ca	Ni	W
1	99.98		0.02			
2	99.28	0.72				
3	70.17	19.44	0.89	6.49	0.35	2.65

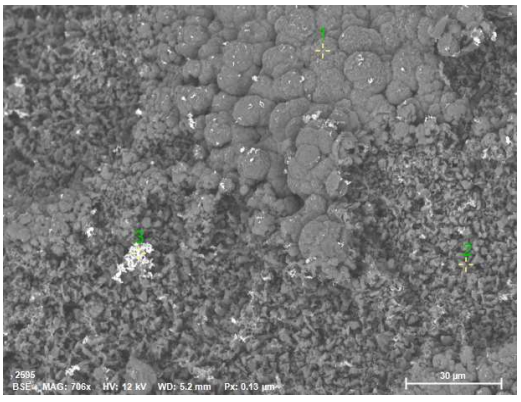

Figure15. Backscattered electrons SEM images of Graphitization Residues sample with the selected points (noted in green) for the EDS analysis and

The EDS analyses of the residues with soft-lamellae shape (Fig. 16 and Table 11) show the highest carbon content. The two analysed points have the percentage of 99.4% and 100% of carbon content.

Table 11. EDS analyses of the Graphitization Residues sample. Atomic concentrations in percentage of the analysed points showed in Figure 16, from spectrum 1 to 2.

Atomic concentration [%]		
Spectrum	C	O
1	99.4	0.6
2	100	

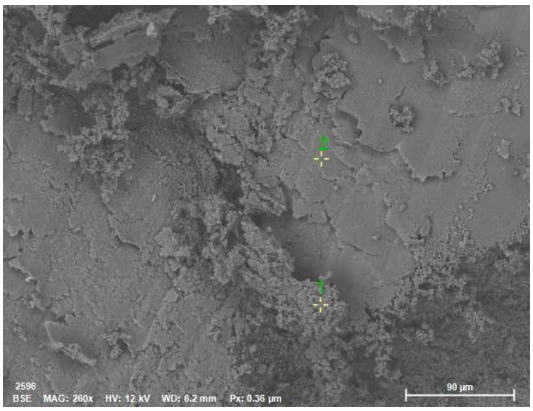

Figure 16. Backscattered electrons SEM images of Graphitization Residues sample with the selected points (noted in green) for the EDS analyses and

4.1.1.5 Graphite before recovery

The SEM images of the Graphite Before Recovery sample (Fig. 17) show angular and layered particles with a homogeneous grain size between 20 and 30 µm. The particles are agglomerated, and it is possible to notice some smaller grains around the biggest particles.

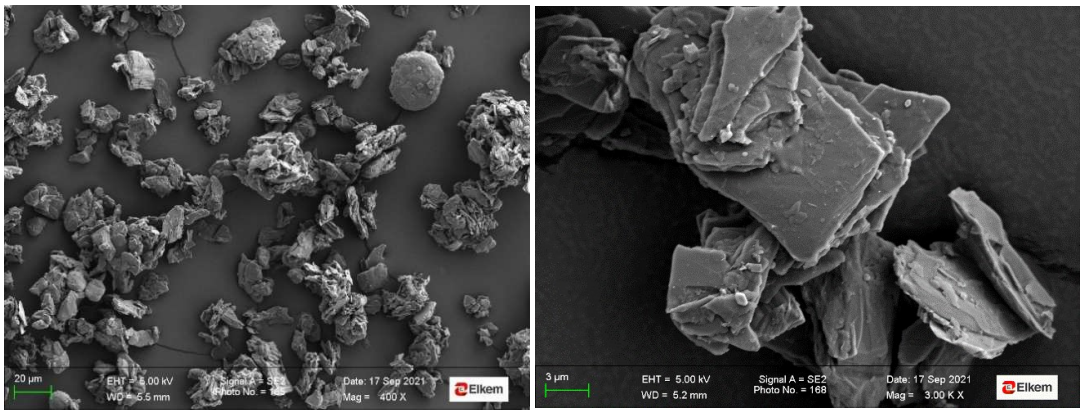

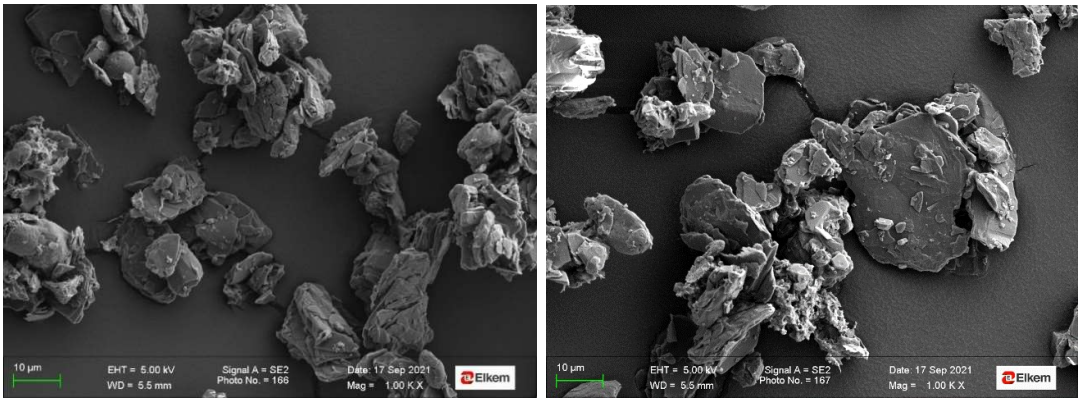

Figure 17. Graphite before recovery SEM analysis

From the BSE (backscattered electrons) images (Fig. 18) it is possible to observe that the smallest particles around the biggest one mentioned above have a whitest colouring. From the EDS analysis (Table 12) is highlighted that their composition (spectra 11, 15, and 16) is not pure carbon which is lower than 77.99%, but there even are oxygen (17.98<O<61.5%), fluorine (just in spectrum 16, 0.58%), alumina (0.37<Al<1.79%), sulphur (1.42<S<5.89), cobalt (0.29% in spectrum 11, and 0.19% in spectrum 15), and nickel (1.29<Ni<4.31).

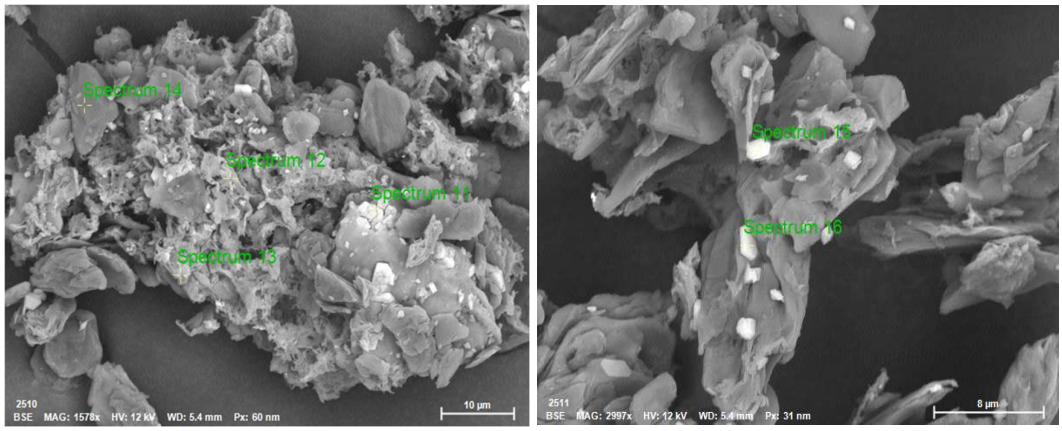

Figure 18. Backscattered electrons SEM images of Graphite before recovery sample with the selected points (noted in green) for the EDS analysis

Table 12. EDS analyses of the Graphite before recovery sample. Atomic concentrations in percentage of the analysed points showed in Figure 18, from spectrum 11 to 16.

Atomic concentration [%]							
Spectrum	C	O	F	Al	S	Co	Ni
11	26.21	61.5		1.79	5.89	0.29	4.31
12	80.79	9.94	7.62	0.66	0.94		0.04
13	84.65	8.53	4.14	0.92	1.63		0.13
14	92.3	5.86	0.86	0.52	0.46		
15	72.2	21.61		0.37	2.39	0.19	3.24
16	77.99	17.98	0.58	0.74	1.42		1.29

4.1.1.6 Graphite after purification

The SEM images (Fig. 19) of the Graphite After Purification sample show a quasi-homogeneous sample made of agglomerates crystals with a visible layered structure but there even are some rounds and not layered particles. It is also possible to observe that even in this sample there are still some smallest particles around the biggest one.

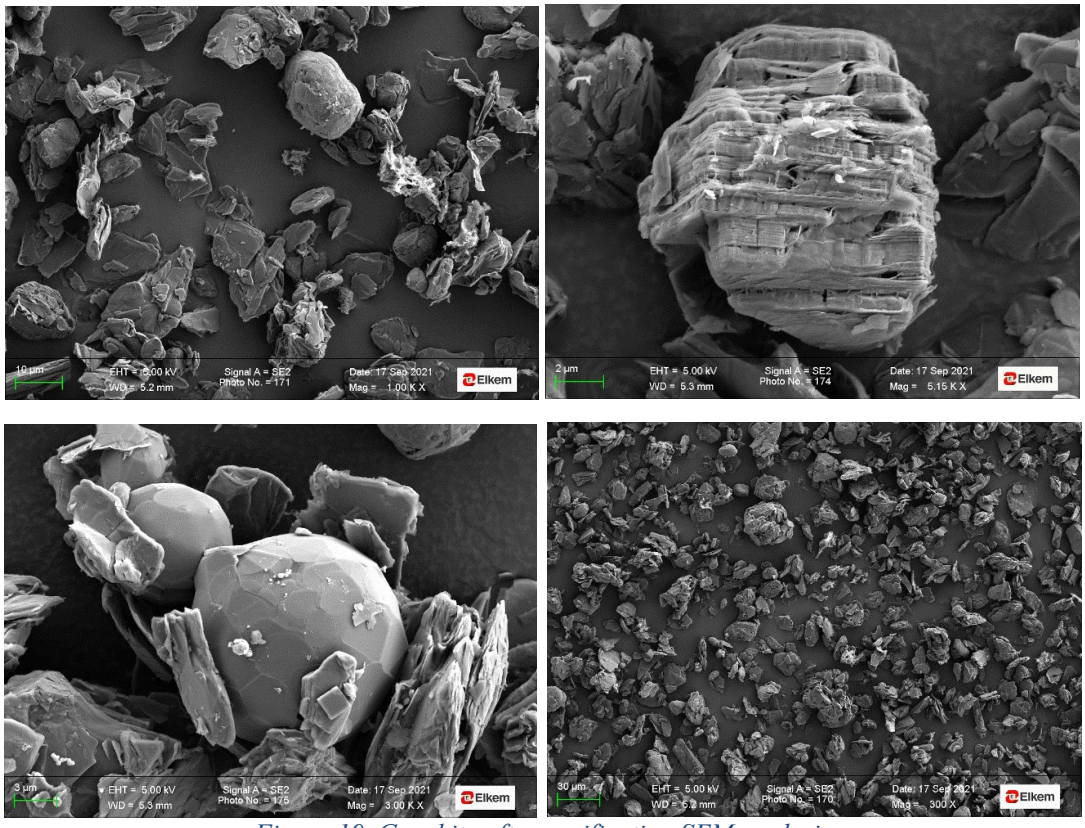

Figure 19. Graphite after purification SEM analysis

The EDS analyses of the Graphite After Purification sample (Fig. 20 and Table 13) show that, except for spectra 19 and 21, which have a lowest carbon percentage respectively 96.57 and 95.33%, the spectra 1, 2, 3, 4, 18, and 20 have a carbon content >98.27 with some impurities made of oxygen (<4.53%), sulphur (<0.11%), sodium (<0.06%), and silica (0.6%).

Figure 20. Backscattered electrons SEM images of Graphite after purification sample with the selected points (noted in green) for the EDS analysis

Table 13. EDS analyses of the Graphite after purification sample. Atomic concentrations in percentage of the analysed points showed in Figure 20, from spectrum 1 to 4 and from 18 to 21.

Atomic concentration [%]					
Spectrum	C	O	S	Na	Si
1	100				
2	98.27	1.71	0.02		
3	100				
4	99.55	0.45			
18	98.3	1.68	0.02		
19	96.57	3.2	0.11	0.06	0.06
20	100				
21	95.33	4.53	0.05	0.04	0.06

4.1.1.7 Graphite after recovery

The SEM images of Graphite After Recovery sample (Fig. 21) show that the particles have a homogeneous grain size between 10 and 20 µm, with soft-angular shape. The grains are the result of crystal agglomeration and thus the layered structure is clear from the pictures.

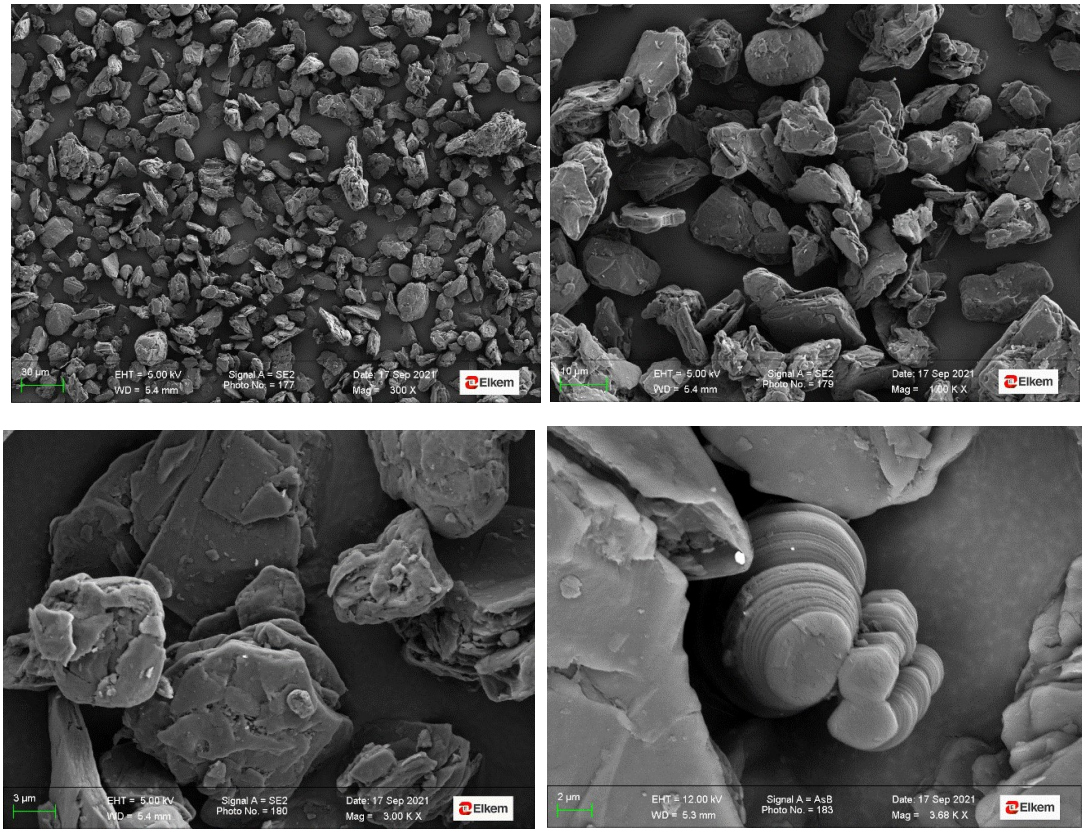

Figure 21. Graphite after recovery SEM analysis

The EDS analyses (Fig. 22, Table 14) of two selected points (spectrum6) of one more layered particle and one withest grain located in the corner of one biggest particle (spectrum 5) show that the whitest particle is a tungsten carbide (C: 96.75 wt%; W: 3.25 wt%), while the more layered particle (spectrum 6) pure carbon composition.

Table 14. EDS analysis of the Graphite after recovery sample. Atomic concentrations in percentage of the analysed points showed in Figure 22 of spectrum 5 and 6.

Atomic concentration [%]		
Spectrum	C	W
5	96.75	3.25
6	100	

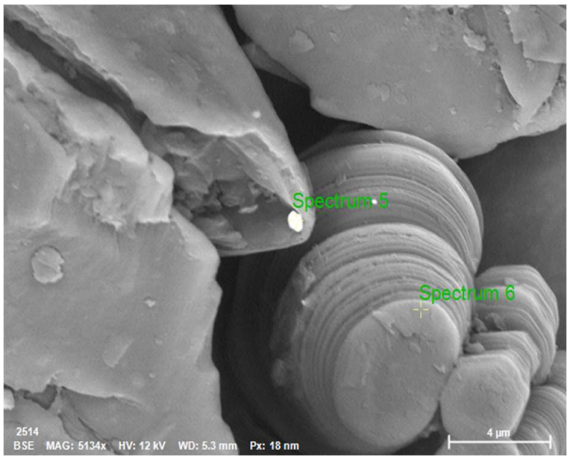

Figure 22. Backscattered electrons SEM images of Graphite after recovery sample with the selected points (noted in green) for the EDS analysis and

4.1.2 XRD

From the XRD analyses I decided to compare the X-ray diffraction pattern of graphite before, during, and after recovery in one graph (Fig. 23) and natural, synthetic, and after recovery graphite in another graph (Fig. 24).

From Figure 23 we can observe that most of the peaks of the three samples correspond to the standard peaks of Graphite 2H (hexagonal) and Graphite 3R (trigonal), respectively the red and black vertical lines. What is very clear is the difference between the black X-ray diffraction pattern and the green and orange ones. The black one corresponds to the graphite before recovery, and it shows a lot of little peaks (from 5 to 39 2θ) with lowest intensities from those of the graphite. These peaks are the detection of the impurities.

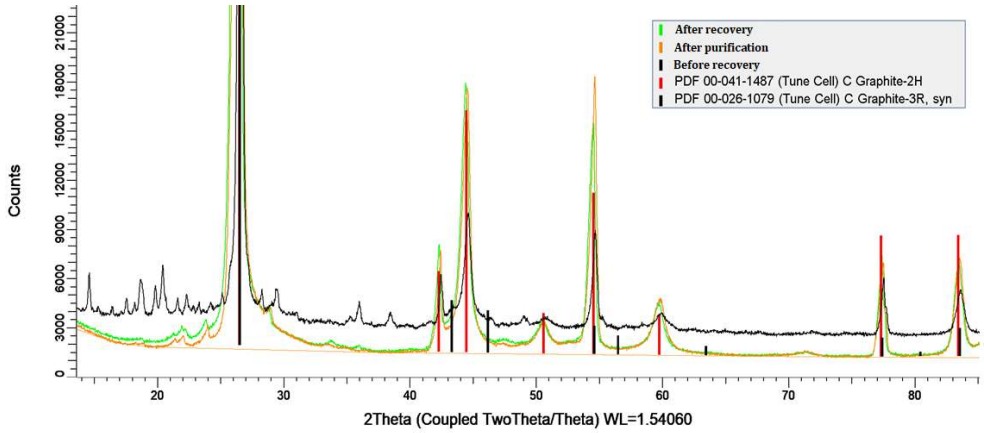

Figure 23. XRD analyses of graphite before recovery (black spectrum), after purification (orange spectrum) and after recovery (green spectrum).

From Figure 24, it is possible to observe that the three different patterns are almost the same, except for a peak of the natural graphite pattern (red) at 43.5 2θ, but it corresponds to a peak of graphite 3R.

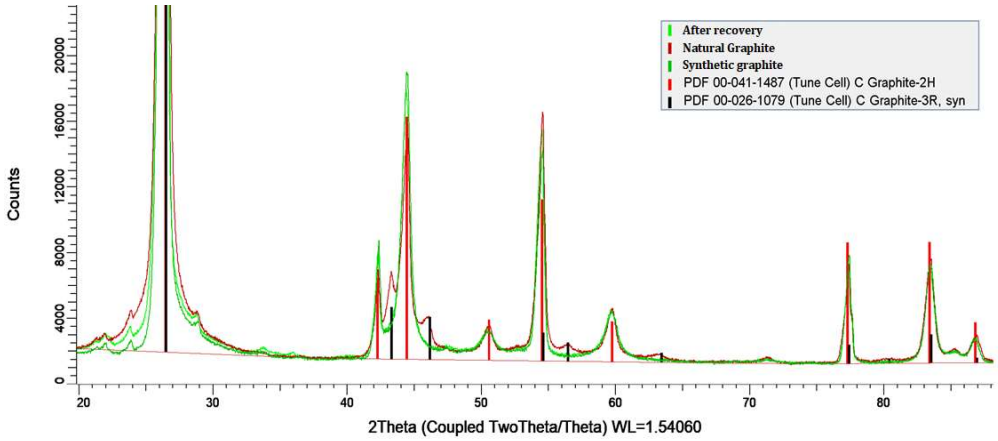

Figure 24. XRD analyses of graphite after recovery (light green spectrum), natural graphite (red spectrum) and synthetic graphite (dark green spectrum).

4.1.3 XRF

The Green Coke XRF analyses (Table 15) shows that the material has high concentrations (ppm) in alumina (334), calcium (607), iron (381), potassium (144), manganese (244), and silica (2723). This last concentration is the highest value of the entire sample. There are even lowest concentrations (ppm) of copper (8), manganese (5), sodium (3), nickel (13), phosphorous (4), titanium (24), and zinc (1). The Synthetic Graphite sample (table 16), instead, shows has high content in vanadium (25ppm), in addition there is evidence of Ca, Cr, Cu, Fe, Na, Ni, and Ti respectively (in ppm) 1, 6, 6, 2, 5, 3, and 8. The natural graphite sample XRF analysis (table 17) shows the presence of Al (5ppm), Cu (7ppm), K (1ppm), Mg (4ppm), Na (4ppm), Ni (1ppm), and Zn (1ppm), with highest content of Fe (22ppm) and Ti (12ppm).

Table 15. XRF analysis of Green Coke.

Green Coke	
Element	Value (ppm)
Al	334
Ca	607
Cr	0
Cu	8
Fe	381
K	144
Mg	244
Mn	5
Na	3
Ni	13
P	4
Si	2723
Ti	24
V	0
Zn	1

Table 16. XRF analysis of Synthetic Graphite.

Synthetic graphite	
Element	Value (ppm)
Ca	1
Cr	6
Cu	6
Fe	2
Na	5
Ni	3
Ti	8
V	25

Table 17. XRF analysis of Natural Graphite.

Natural Graphite	
Element	Value (ppm)
Al	5
Cu	7
Fe	22
K	1
Mg	4
Na	4
Ni	1
Ti	12
Zn	1

As regards the recycling process, the Graphite Before Recovery XRF analysis (Table 18) shows very high percentage of Al (6801ppm), Mn (615ppm), Cu (498ppm), P (296ppm), and Si (209ppm). In addition, there is lower content of calcium, iron, potassium, sodium, and titanium, respectively (in ppm), 4, 20, 2, 69, and 15. Then, in the Graphite After Purification sample, the ppm concentrations significantly decrease, the highest ppm content is the one of iron (60 ppm), even if there is a high amount of titanium (35 ppm). The Graphite After Recovery sample, instead, shows an additional decrease of the values in ppm, titanium reaches 11 ppm and iron 40 ppm.

Table 18. (Left) XRF analysis of Graphite Before Recovery, (Centre) XRF analysis of Graphite After Purification, (Right) XRF analysis of Graphite After Recovery.

	Before Recovery	After Purification	After Recovery
	Values in ppm		
Al	6801	3	5
Ca	4	8	
Cr		3	1
Cu	498	7	7
Fe	20	60	40
K	2		1
Mn	615	1	1
Na	69	7	
Ni		5	3
P	296		
Ti	15	35	11
Si	209		
V		7	2
Zn			1

4.1.4 TEM

4.1.4.1 Natural Graphite

The figure below (Fig. 25) shows the selected particle for the TEM sample preparation (FIB) and subsequently, for the TEM analysis. It presents a round and irregular shape with a flat-flakes surface. The particle has been chosen because it represents well the whole sample particles morphology (see Fig. 8).

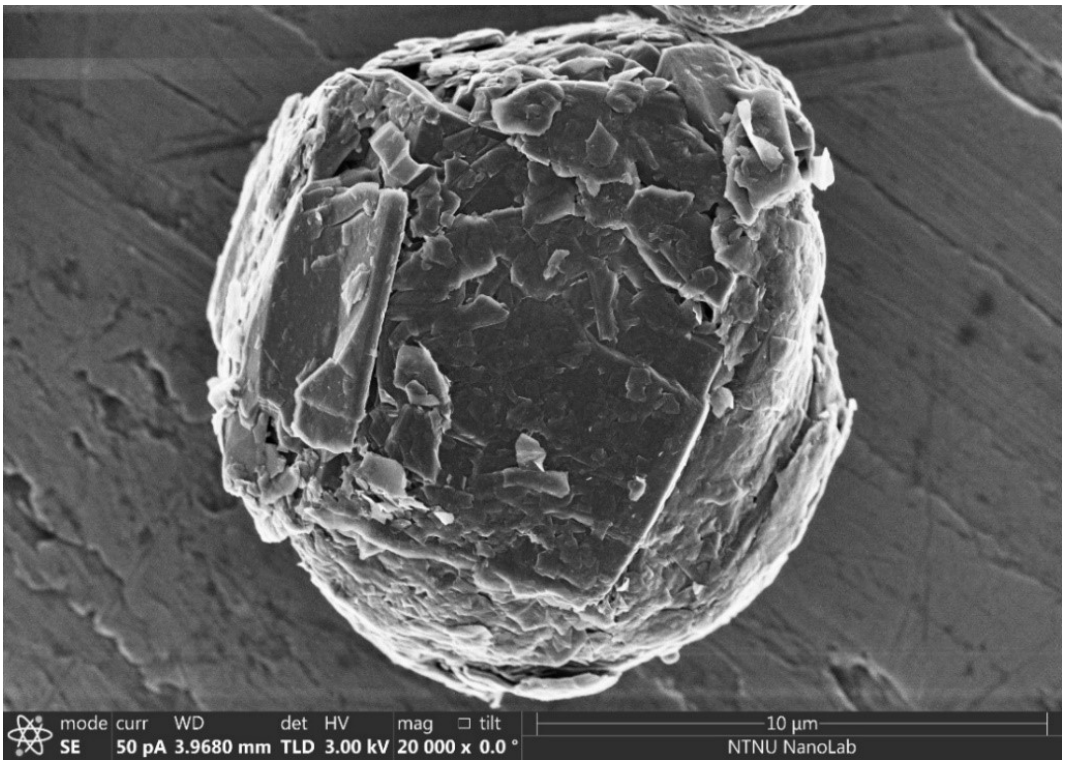

Figure 25. Secondary electron SEM image of natural graphite sample. Magnification of 20k X.

From Figure 26, it is possible to observe the section and internal structure of the selected particle showed in the previous picture (Fig. 25) at a magnification of 8000 x. The sample is made of different macro-layers separated and surrounded by white zones and arranged in a spiral and angular shape.

From Figure 27, instead, it is possible to observe the internal structure of the particle at magnification of 120k X, and even in this case, the layered structure remains preserved on a large scale, but even on a small scale. It is noticed that the sample section under TEM analyses at bright field imaging creates striations of dark and light colours at least with three orientations, one from top left to lower right, another one with the same direction but with a different immersion angle, and the last from lower left to top right. This coexistence

of different layer orientations in a small part of the sample obviously causes an overlap of them, and in one case it is possible to observe a point of suturing/contact of syn-growth.

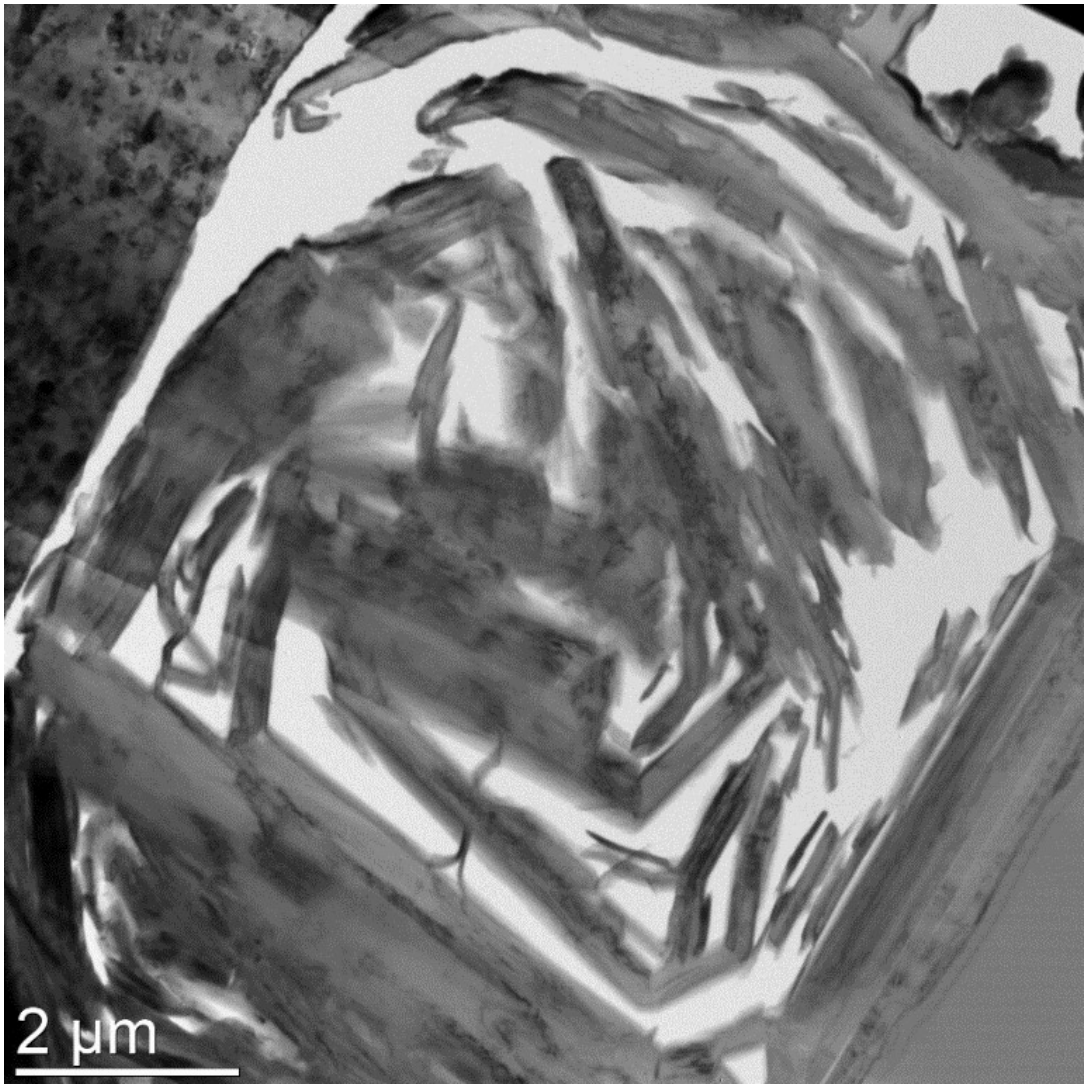

Figure 26. TEM image of a natural graphite particle section originated by FIB. Magnification of 8k X, Bright Field (BF) imaging.

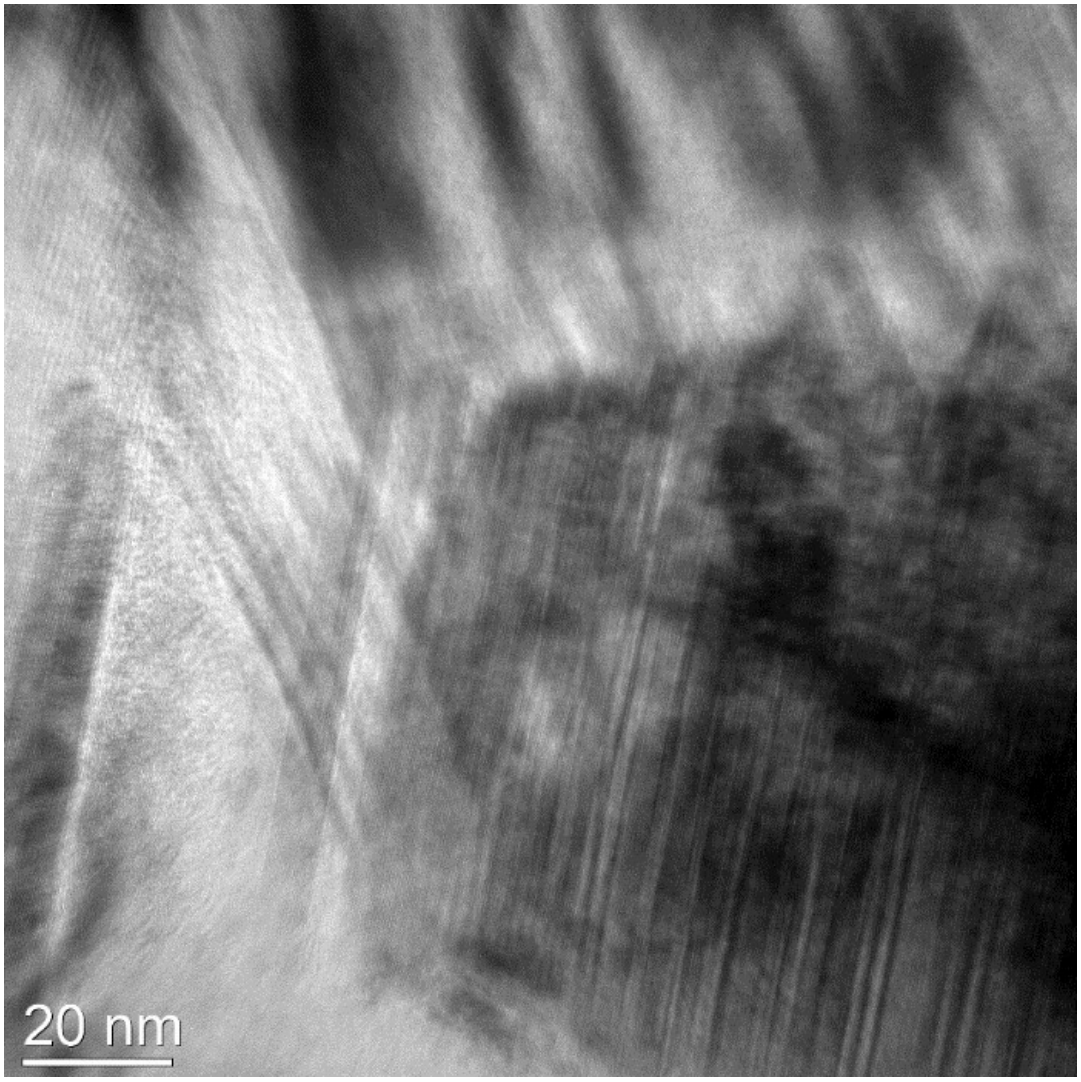

Figure 27. TEM image of a natural graphite particle section originated by FIB. Magnification of 120k X, Bright Field (BF) imaging.

Figure 28 shows the same sample but with a 200k X magnification. In this case, there are three different zones: the first one is in the upper part of the picture, and it presents a preferred orientation of the layers from lower left to upper right, but moving to the right, the layers present curved, soft, and not defined lines; the second zone is located in the centre of the picture and it can be defined as the separator of the zones above and below. The central zone is linear/sub-curve, with a constant thickness, and the separation between the two other zones is clear because of darker and strain lines between them. The third zone, below the central one, is made up of two-layer orientations that seems to be overlapped, the first layers have an orientation from lower left to top right, while the second layers have an orientation from lower right to top left. The contacts between the central

zone and the upper and lower parts are quite different: the upper part has a less defined contact caused by the curvature that the contact takes towards the left, while the lower part has a clear and more defined contact.

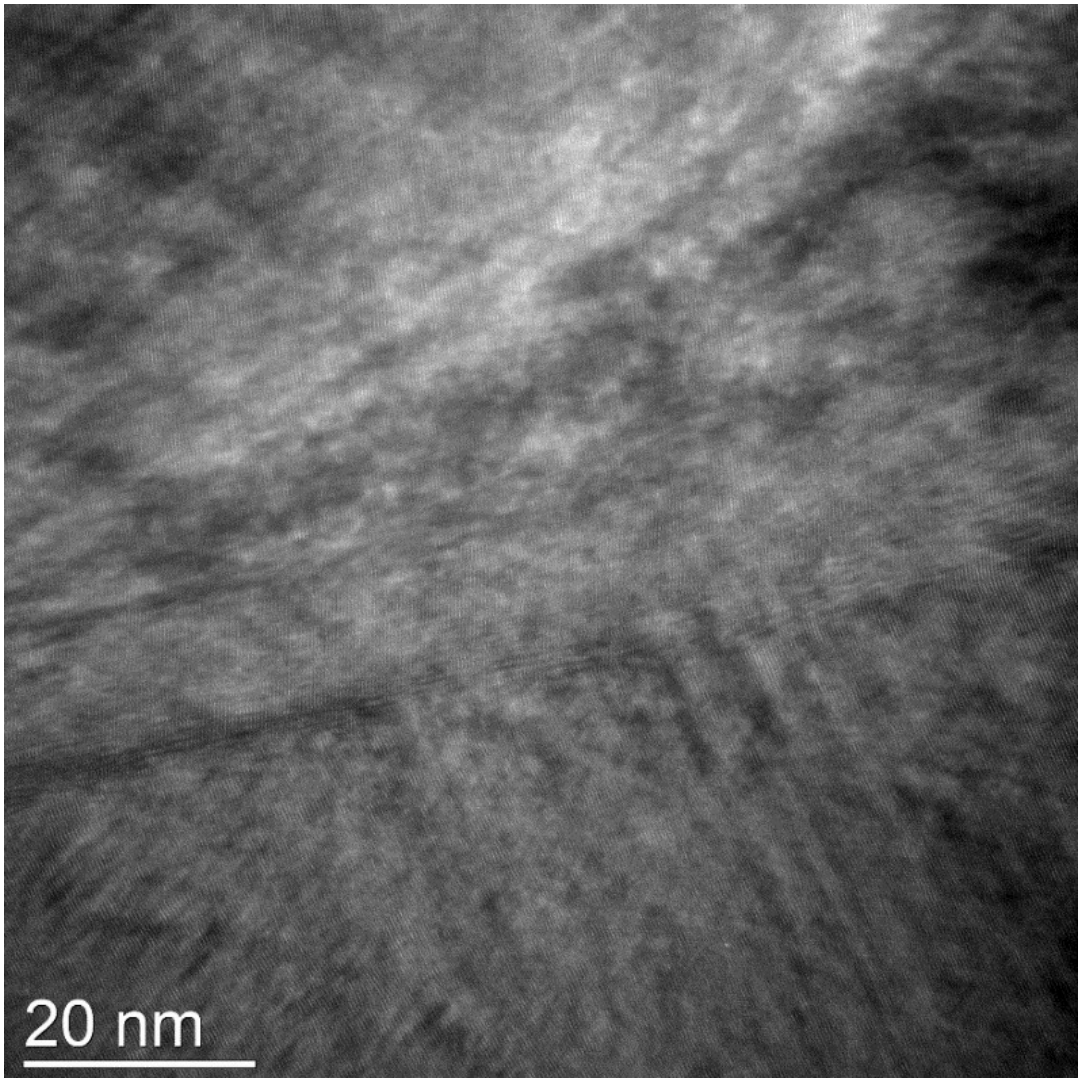

Figure 28. TEM image of a natural graphite particle section originated by FIB. Magnification of 200k X, Bright Field (BF) imaging.

4.1.4.2 Synthetic Graphite

Figure 29 shows the selected particle for the TEM analysis before the sample preparation with the dual-beam focused ion beam (FIB). The particle has angular, sharp, and flat shapes. It has a platy morphology and shows superposed stacks of graphite layers. The section cut by the FIB and analyzed by TEM microscopy is the one extending from the top to the lower part of Fig. 29 and cuts perpendicularly the picture.

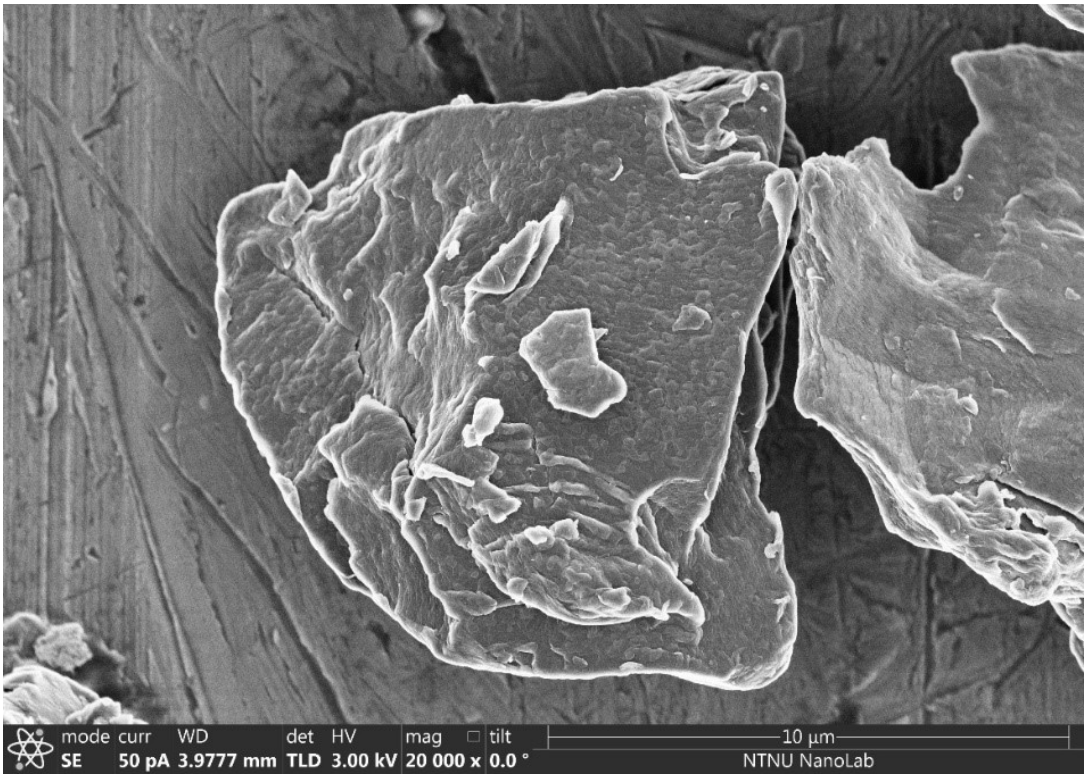

Figure 29. SEM image of Synthetic Graphite sample. Magnification of 20k X.

From Figure 30 it is possible to observe the section of the sample in exam at a magnification of 8000 X. The section has a drop shape and presents the layers with a main orientation from top right to lower left of the picture.

In the lower left part of the picture there is a homogeneous zone composed by a thick layer that surrounds the sample. This layer is composed by two different layers, the thinner one (0.1 µm) is darker, and it is in contact between the sample and the outer layer that is thicker (2 µm), and it has a lighter grey colour. The first layer is the result of the deposition of carbon and hydrogen by the electron beam during the FIB, while the second one is the result of deposition of carbon, hydrogen, and gallium by the ion beam during the FIB. The opposite dark and thin layer around the sample is the result of the re-deposition caused by the ion and electron passage through the sample during the ion and electron beam deposition.

As regards the internal structure of the sample, it is possible to observe that not all the layer lines are continuous and that there is an evident discontinuity of them in the lower left part of the sample picture.

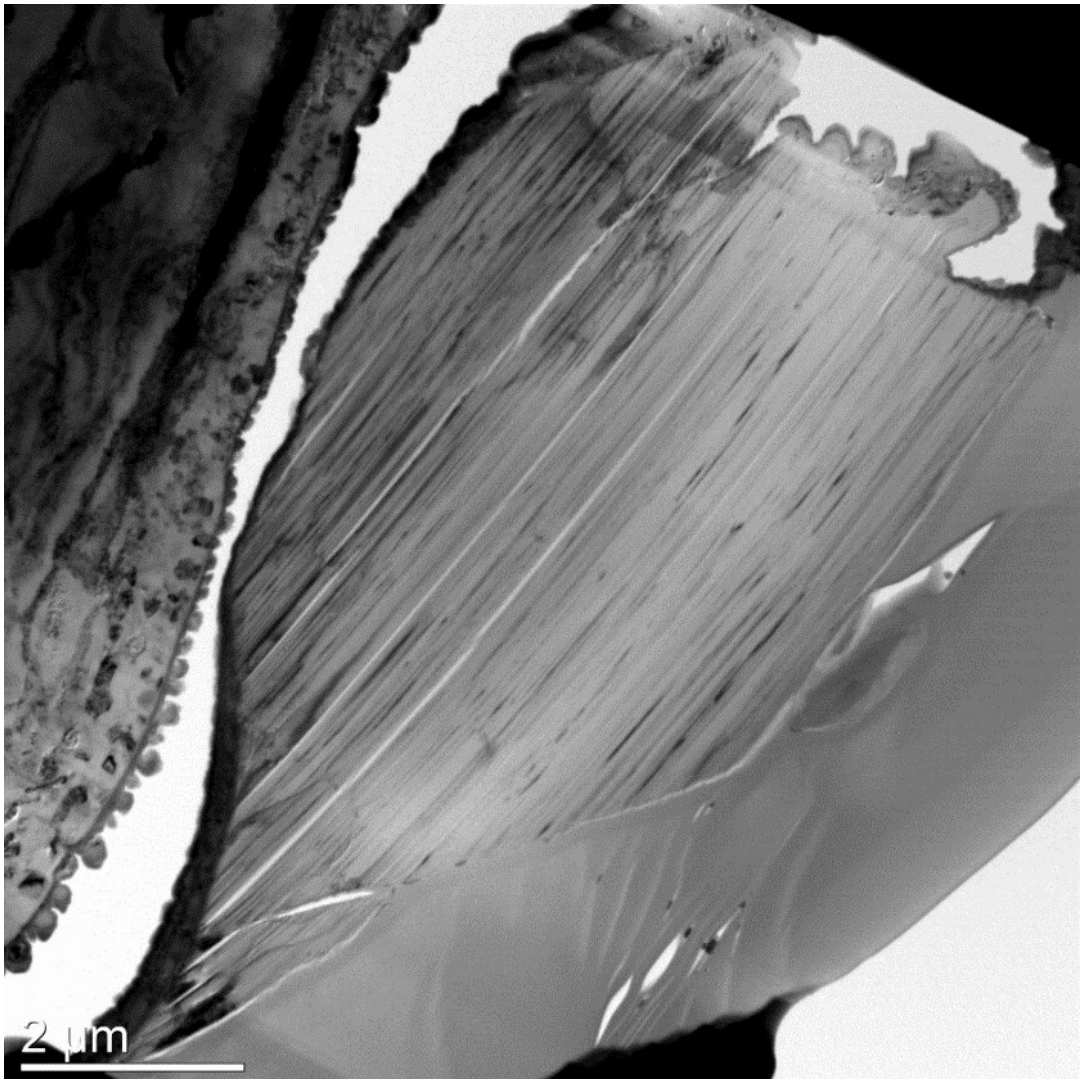

Figure 30. TEM image of a Synthetic Graphite particle section originated by FIB. Magnification of 8k X, Bright Field (BF) imaging.

From Figure 31, the sample is at magnification of 15k X, and the discontinuities are more evident. Their orientation go obliquely from top left to lower right and the deformation lines are less evident than the natural graphite sample. This is caused to the unconformity of the layers in the vicinity if the dislocations.

Instead, from figure 32, it is possible to observe one dislocation at the magnification of 250k X that makes possible the observation of the atomic configuration of the zone. At first impact, it is evident a thumbprint configuration of the atoms in the central part of the picture. In this case, the atoms are arranged in a semi-circular shape that ends to the lower right, where the discontinuity continues obliquely. It is possible to observe the deformation line thanks to a whitest halo, which is dislocated in the middle part, and this is evident because of the different atomic orientation in the outer border of the deformation zone.

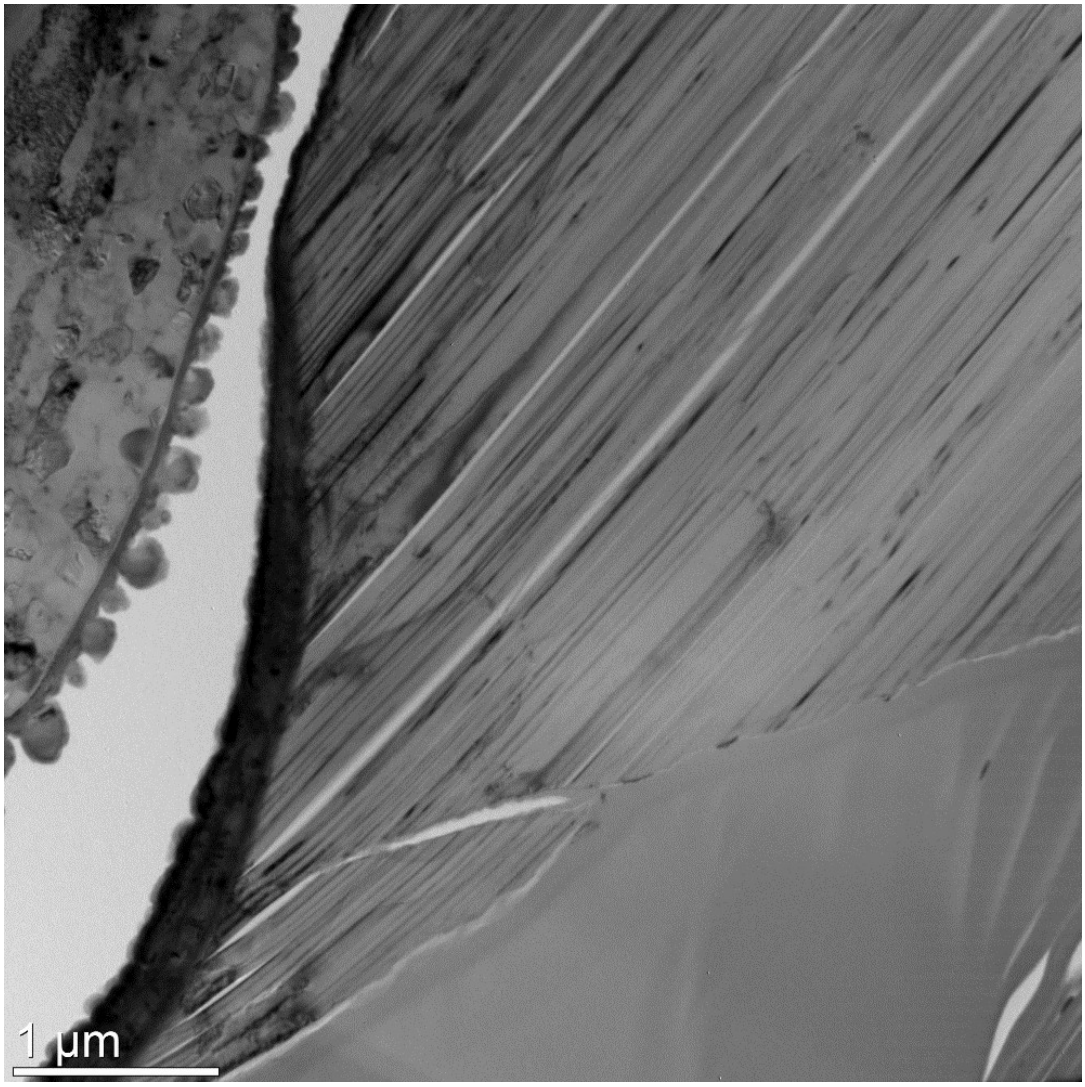

Figure 31. TEM image of the Synthetic Graphite particle section originated by FIB. Magnification of 15k X, Bright Field (BF) imaging.

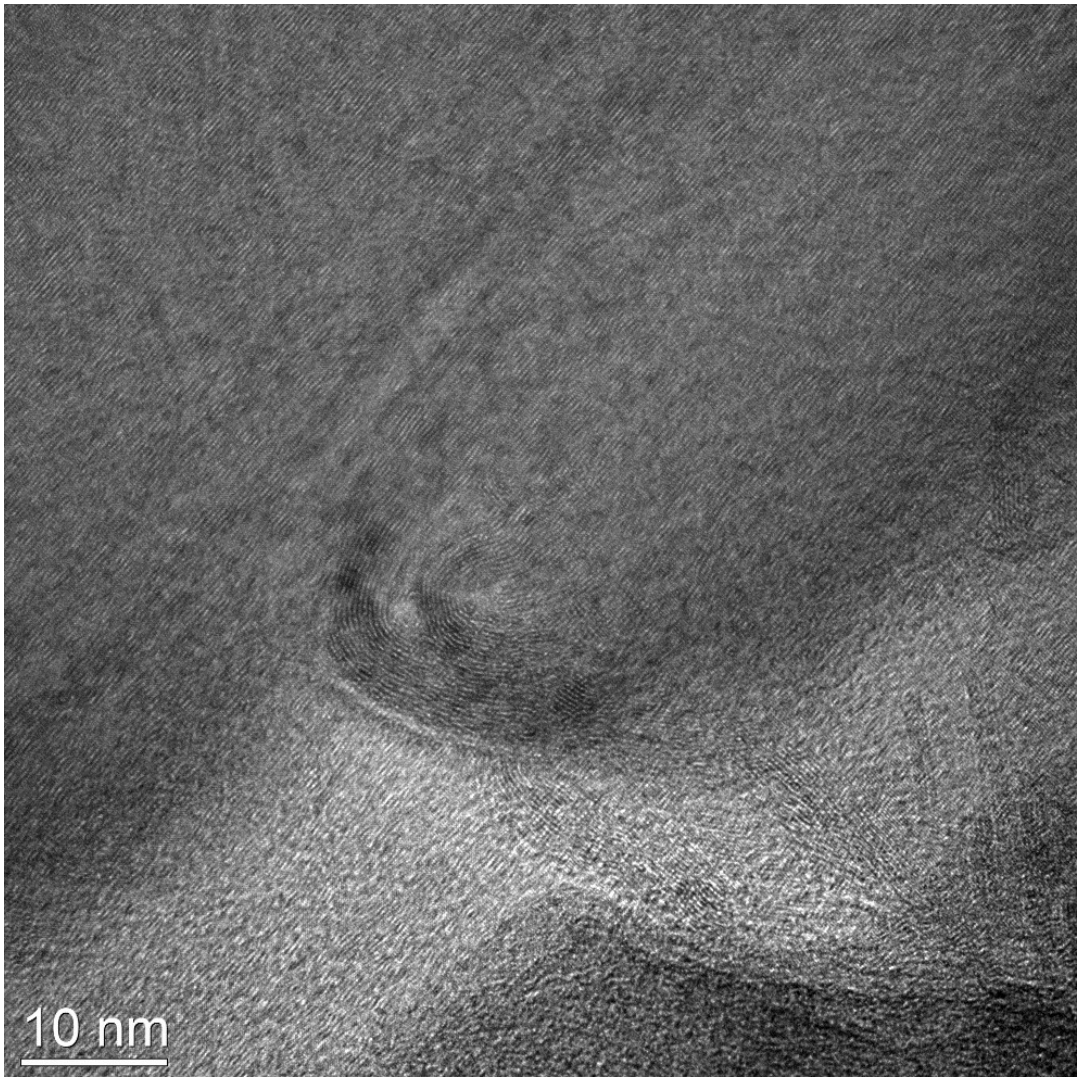

Figure 32. TEM image of the Synthetic Graphite particle section originated by FIB. Magnification of 250k X, Bright Field (BF) imaging.

4.1.4.3 Graphite After recovery

Figure 33 represents the selected particle for the TEM analysis before the sample preparation with the dual-beam focused ion beam (FIB). The particle has a polygonal shape, and it is possible to notice that it presents different levels/layers to the left and right parts which gives to the particle a non-flat shape to the top (towards to the observer).

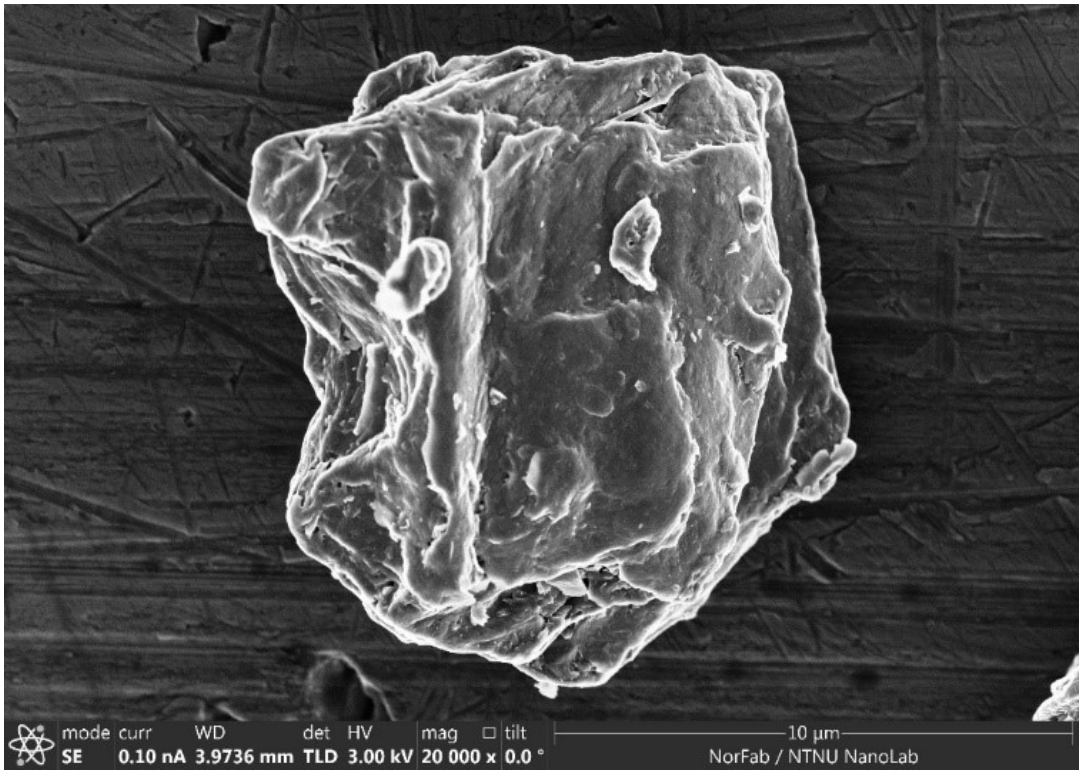

Figure 33. SEM image of Graphite After Recovery sample. Magnification of 20k X.

Figure 34 shows the TEM overview bright field (BF) image of the selected particle for the structural analysis. From the picture is it possible to notice that around the particle there are two different layers, the first one light-grey and the second one dark-grey and thicker. The cause of the formation of these layers is the same as the sample of synthetic graphite (Fig. 30), thus the deposition of carbon and hydrogen for the first layer and carbon, hydrogen, and gallium for the second layer. Instead, as regards the darker zone around the opposite side to the grey layers, it is the results of re-deposition of H-C-Ga during the ion and electron beam action.

The section of the sample shows a complex system of layers and empty lenses (white parts) that are oriented approximately from the top to the lower part. These layers are affected by the passage of several deformations which cut the *a*-axis in different parts.

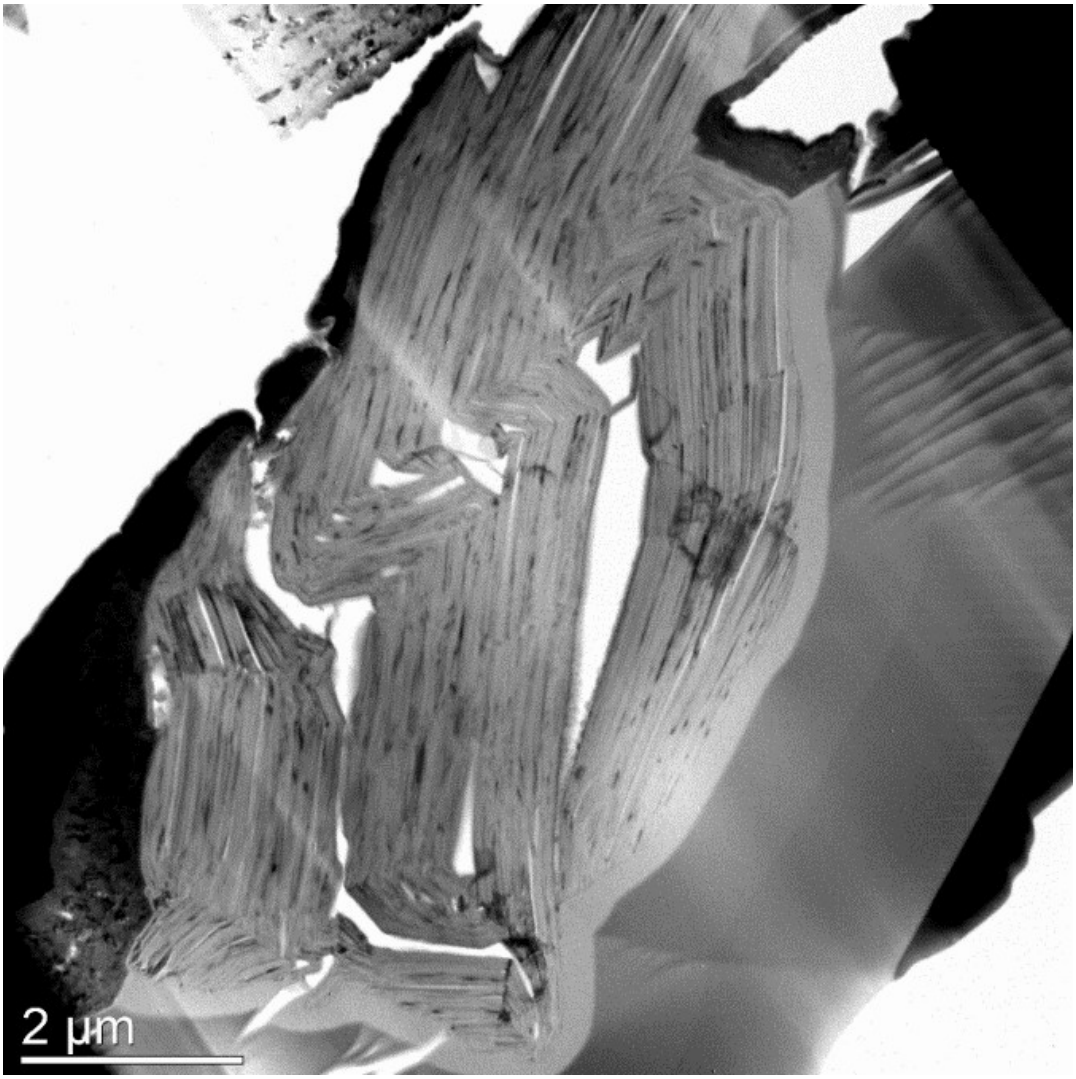

Figure 34. TEM image of the Graphite After Recovery particle section originated by FIB. Magnification of 8k X, Bright Field (BF) imaging.

From Figure 35, it is possible to observe one of the dislocation zones present in the sample at a magnification of 12k X. The dislocations in the picture are four, but the most evident is the one in the upper part that cut the section in diagonal. The dislocation in exam is evident thanks to some layer discontinuities and thanks to some suture between those layers without discontinuity. In addition, there is a particular zone in the left part of the discontinuity which assume a triangular shape. In this triangular zone, the layers have a different orientation thank the whole sample.

From Figure 36, the deformation zone is zoomed at a magnification of 100k X, and it is possible to observe that the dislocation is not a simple contact surface, but it is composed by an entire area of deformation which is located between the two parts of the sample

with different forces. From figure 37, the same dislocation is zoomed at a magnification of 400k X, and it is possible to observe better the dislocation zone at atomic scale.

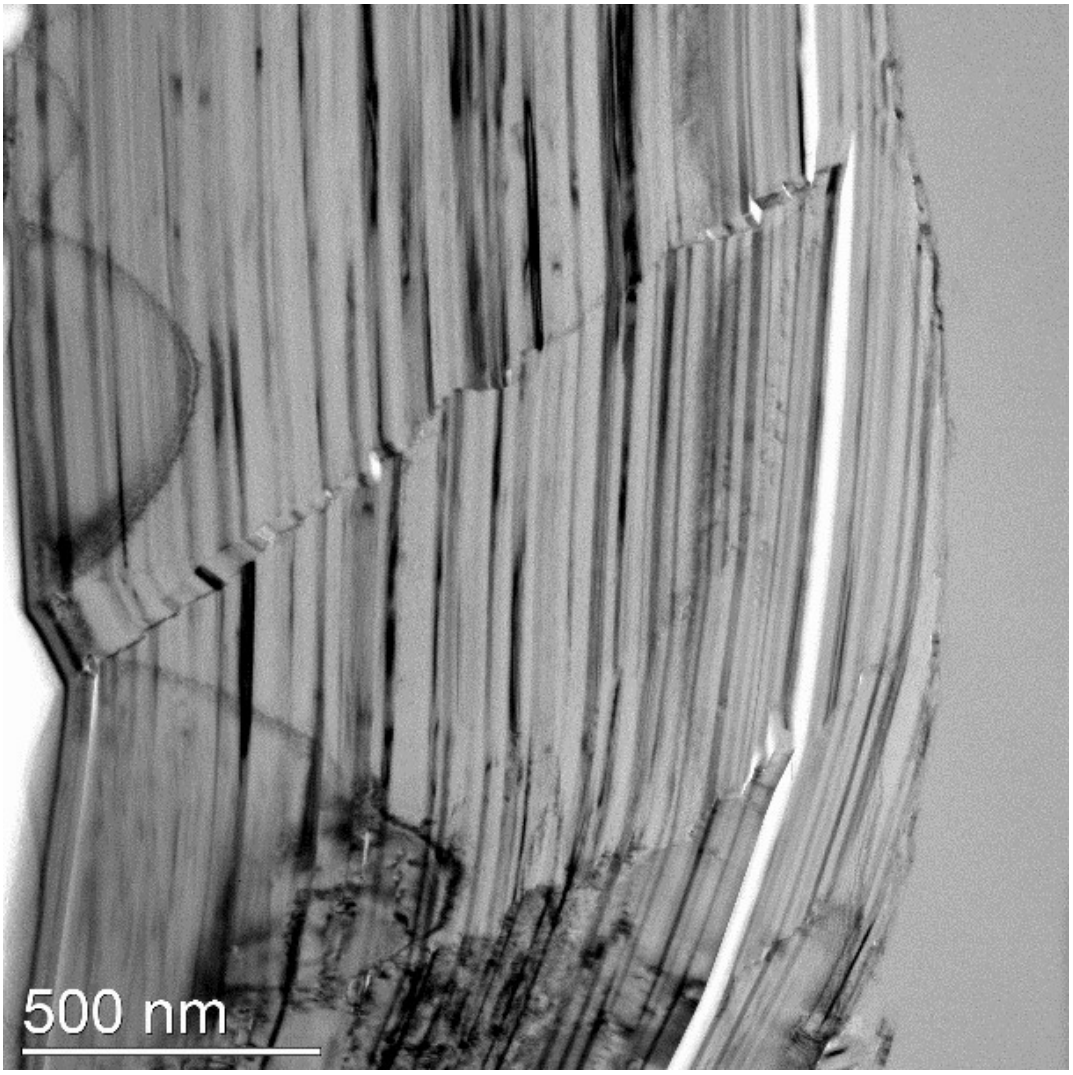

Figure 35. TEM image of the Graphite After Recovery particle section originated by FIB. Magnification of 12k X, Bright Field (BF) imaging.

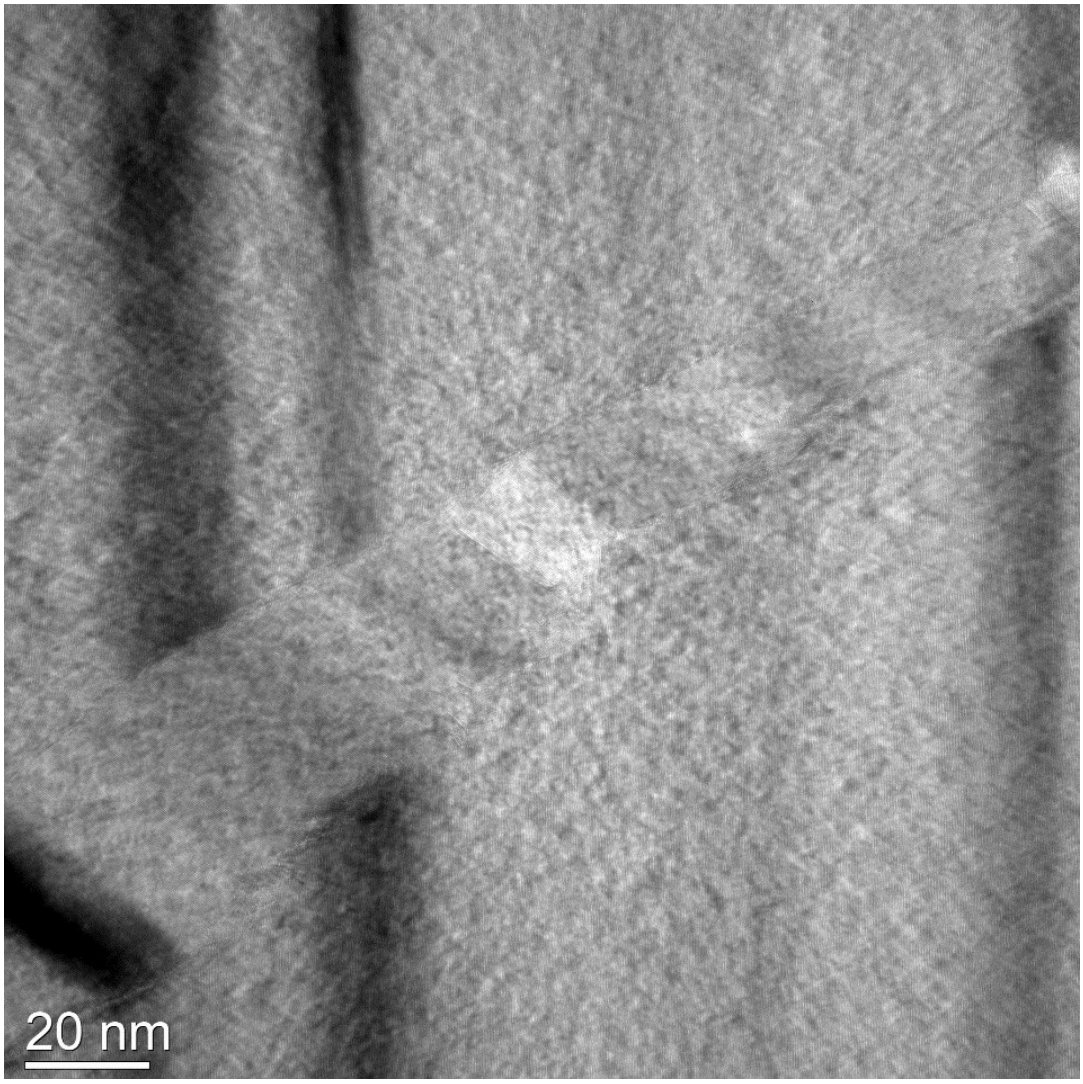

Figure 36. TEM image of the Graphite After Recovery particle section originated by FIB. Magnification of 100k X, Bright Field (BF) imaging.

At a magnification of 400k X (Fig. 37), it is possible to observe the atoms distribution in the dislocation zone. The picture can be divided into three parts separated by two lines with a chaotic atomic texture (obliquely from lower left to upper right). These three parts are characterized by their different orientation of the layers: the upper and lower parts have a sub-vertical orientation, while the central part is characterized by an oblique, from top left to lower right, orientation.

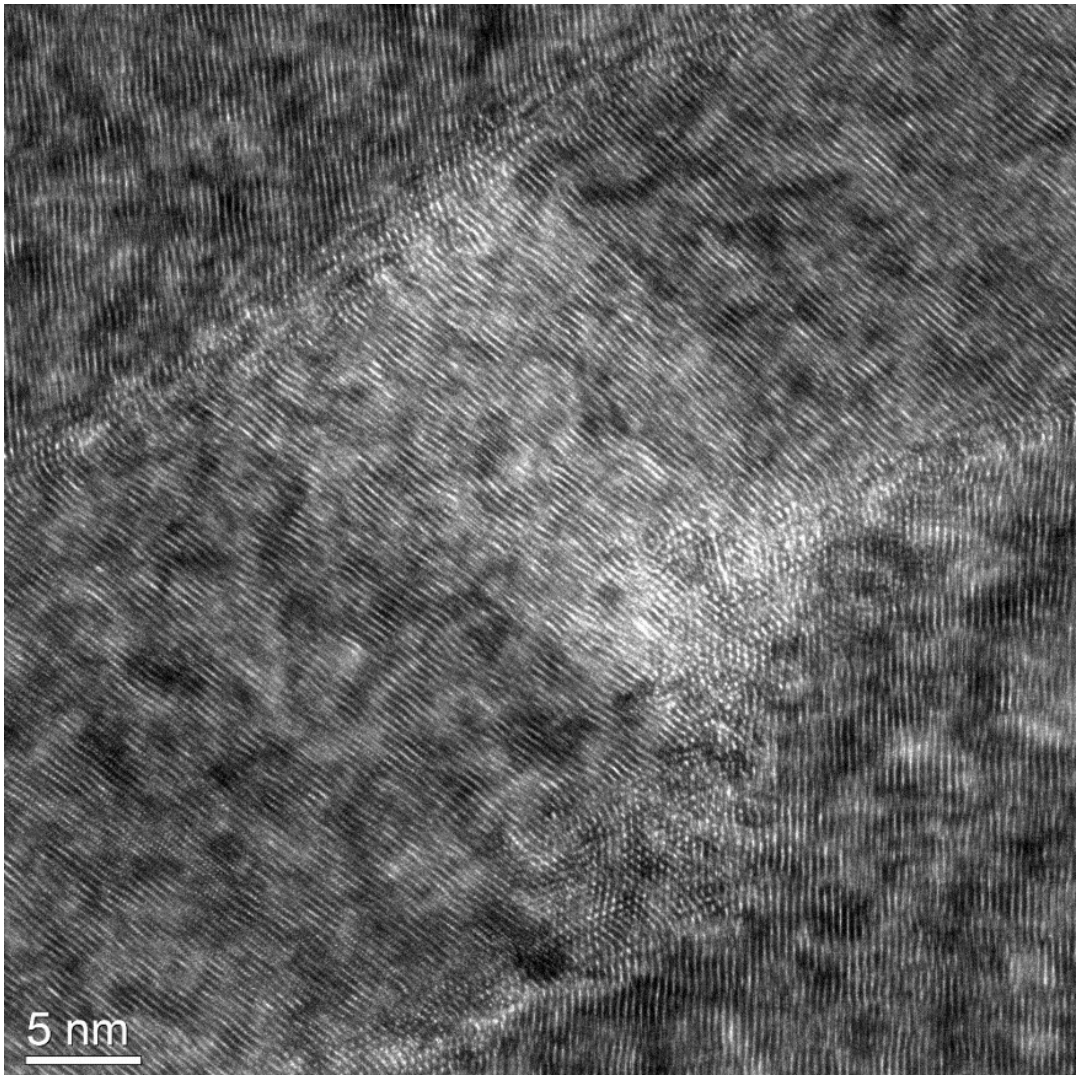

Figure 37. TEM image of the Graphite After Recovery particle section originated by FIB. Magnification of 400k X, Bright Field (BF) imaging.

4.2 Material Flow Analysis

4.2.1 Current graphite flow and Baseline scenario

From Figure 39 it is possible to observe the current graphite flow for the year 2021. The equations for the quantifications are shown in the appendix. The numbers in yellow rectangles represent the mass of graphite material, while the numbers in grey rectangles represent the mass of carbon relatives to the number in the yellow box of the same flow.

As explained before, the current graphite flow does not include the graphite recycling, for this, the values of mass of graphite material and mass of carbon content are equal to zero from flow A10-12 to flow A15-3 (Fig. 39). The graphite flow in the 2021 consists of synthetic graphite and natural graphite production and mixing (process 3, Fig. 39), then

the mix is used in order to produce the anode material for EVs' LIBs, and after the dismantling of the EOL EVs the graphite material is wasted with the pyrometallurgical process (process 11, Fig. 39). This system, without the recycling processes, is the same used in order to quantify the baseline scenario.

Figure 38 shows the trend results of the flows A0a-1 (coke), that represents the require coke, A1-3 (SY for EVs) that represents the required SY, and A2-3 (Recycled graphite for EV production) that represents the required natural graphite, and flow A0a-2 (natural graphite from mines) that represent required raw NT, quantification of the baseline scenario from 2021 to 2050. Since the percentages of synthetic and natural graphite are 50% and 50% in anode materials for lithium-ion batteries for electric vehicles (from Elkem), their values in Figure 38 are the same, and the requests of these two types of graphite in 2050 is above 3500 kt, while the demand of green coke will be more than 6000 kt. It is even possible to observe that the raw natural graphite demand directly from the mines has the higher values, and in 2050 it will reach the peak of more than 7000kt.

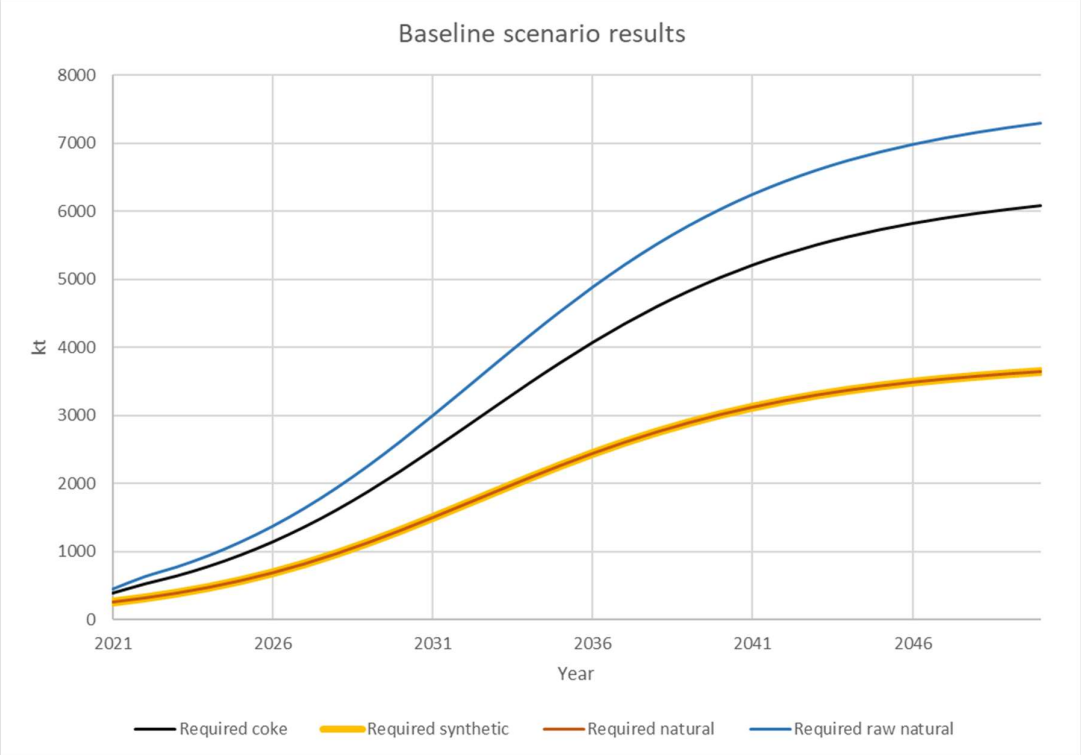

Figure 38. Scenario A. Evolution of coke (black line), synthetic graphite (red-dotted line), and natural graphite (blue line) requests up to 2050. x-axis years, y-axis (kt of material)

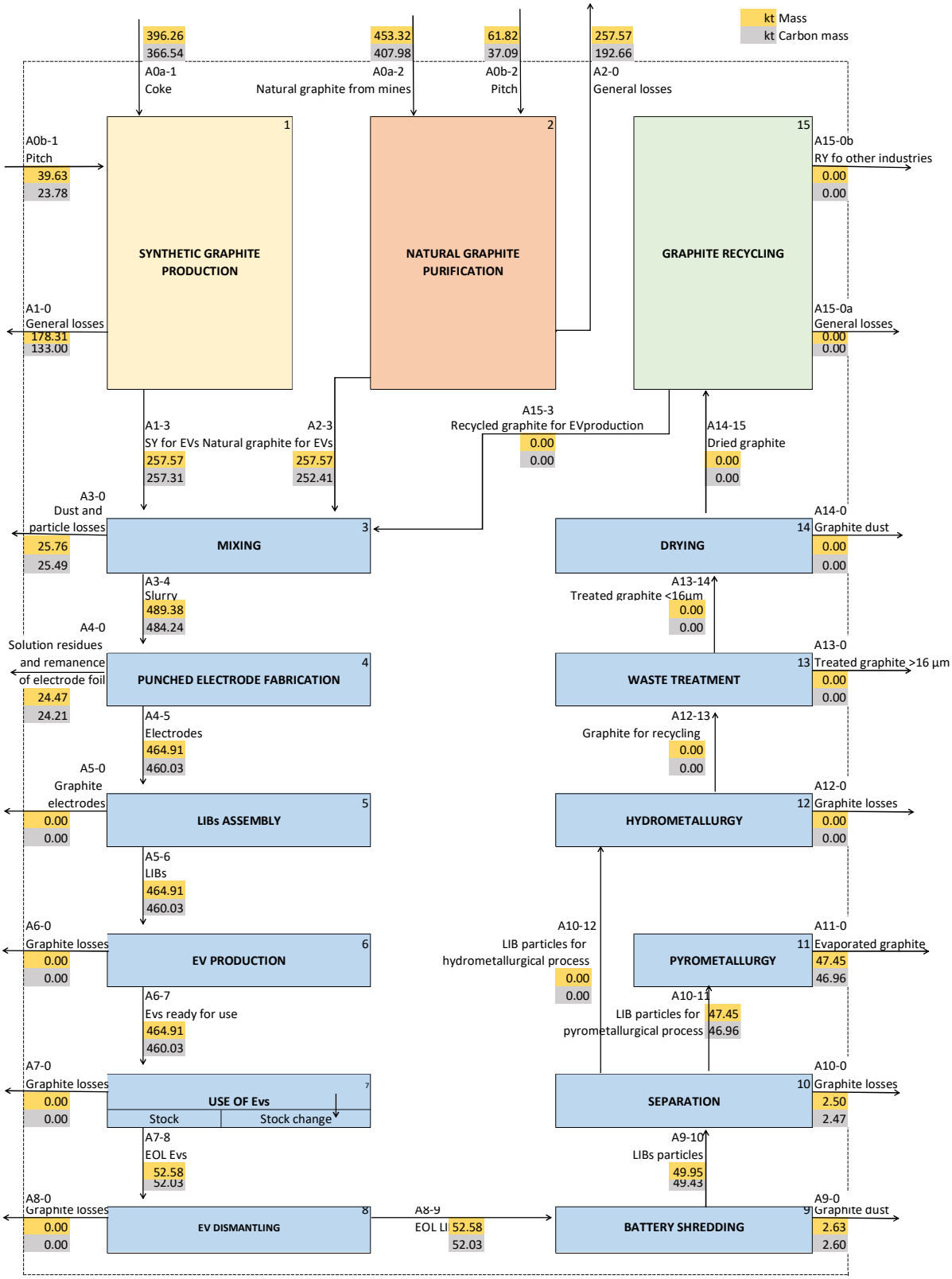

Figure 39. l Current graphite flow system (2021). Light yellow box: synthetic graphite (SY) production; Red box: natural graphite purification; Green box: graphite recycling; Blue boxes: LIBs and EVs production, dismantling, and graphite treatment for a possible recycling. Numbers in yellow rectangles: Graphite Mass; Numbers in grey rectangles: Carbon mass.

4.2.2 Scenarios B, C, and D

Figure 40 shows the plotted results of flows A0a-1 (coke) and A1-3 (SY for EVs) of scenarios B, C, and D up to 2050 compared to the baseline scenario. Up to 2050, the baseline scenario shows lowest values of synthetic graphite and coke demands than the scenarios that include the graphite recycling process. The cause of these differences is related to the fact that for the baseline scenario the synthetic graphite is mixed with the natural one in equal proportions, while in the other three scenarios, the recycled graphite replaces the natural one. Thus, the substitution of the recycled graphite to the natural one, causes an increase of synthetic graphite and coke demand because the graphite doomed to recycling is not enough to fill the shortcomings of natural graphite.

With regard to scenario B (100% recycled and used), and D (gradual recycling, 100% for LIBs) the increasing of the synthetic graphite and coke reach a peak in 2042/2043, but after that, the values decrease again until little bit above the values of the baseline scenario. Instead, as regards scenario C (100% recycled, gradual use for LIBs), the values increase until 2042/2043 but they continue to increase with moderation.

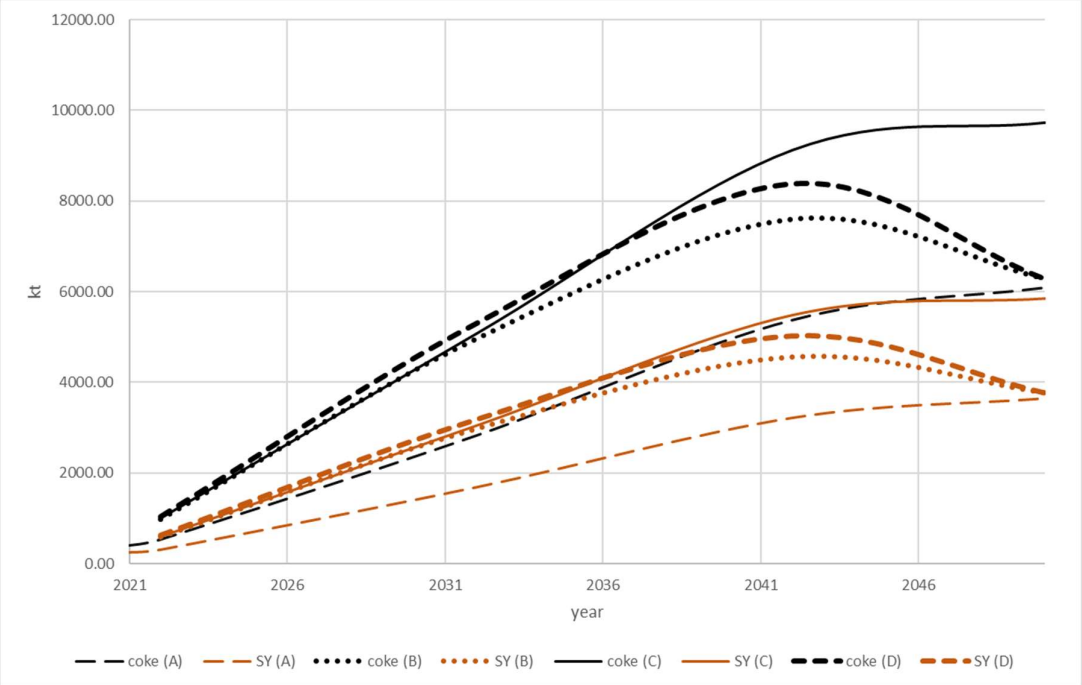

Figure 40. Evolution of coke: black lines, and synthetic graphite (SY): red lines, demand up to 2050 in scenarios A (thin dashed lines), B (dotted lines), C (continue lines), D (thick dashed lines). x-axis years, y-axis (kt of material).

In general, the trends of the three scenarios that includes the recycling process, B, C, and D, show that the values of required synthetic graphite, and consequently coke, are almost twice that of the corresponding baseline scenario since 2042/2043. Except for scenario C, which shows a constant increase of synthetic, and coke demands even after 2042/2043. Instead, scenarios B and D shows that in 2050 the synthetic and coke demands will almost the same as scenario A, but the effort in the past year until today are the double.

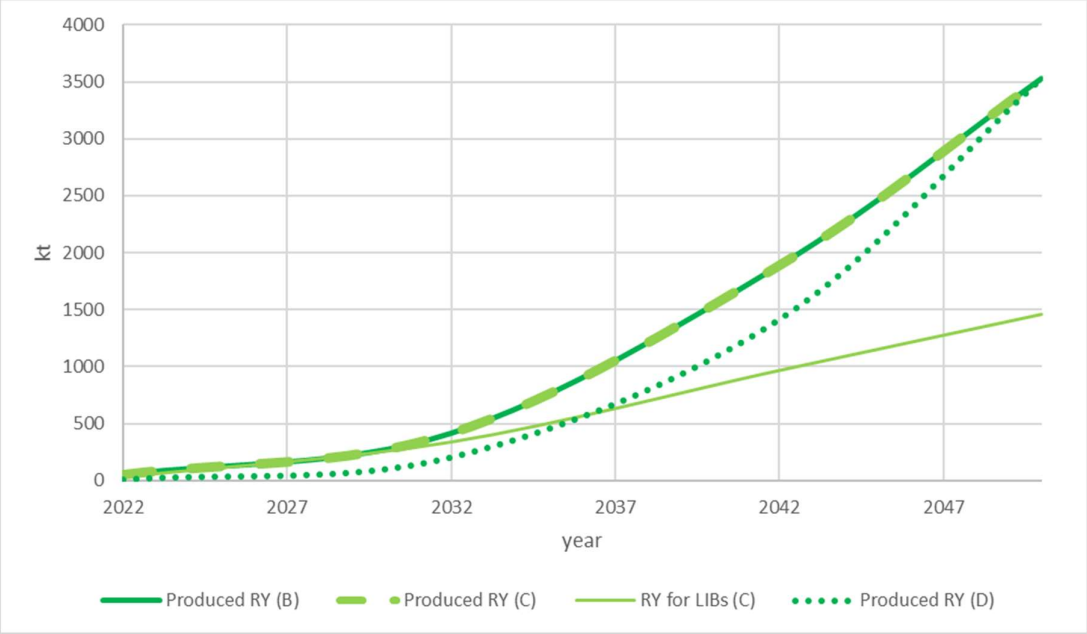

Figure 41. Evolution of recycled graphite (RY) production up to 2050 in scenarios B (dark green and continue line), C (light green dashed line), D (dark green dotted line), and evolution of produced recycled graphite for LIBs in scenario C (light green continue line). x-axis years, y-axis (kt of material).

From Figure 41, it is possible to observe the amount of recycled graphite up to 2050 for the three different scenarios that include the recycling process (B, C, and D).

As regards the produced recycled graphite, from scenario B (dark green plot, Fig. 41), in which all the graphite from anode in the world is recycled and used for EVs' LIBs, it is possible to observe that the recycled graphite production increases very slowly until 2032 because of the cars at the EOL which are not enough at the moment since the EV market is relatively new and young. Then, after the 2032, the produced recycled graphite has a quite rapid increase by reaching more or less 3500 kt in 2050. In addition, comparing the graph in Figure 41 to the one in Figure 40, it is possible to observe that the synthetic graphite required in scenario B (dotted red lines, Fig. 40), follows an opposite trend

compared to the produced recycled graphite (dark green line, Fig. 41). These two opposite trends, in which the produced recycled graphite has a slow increase until 2032 and the synthetic graphite demand has a rapid increase until 2042/2043, are related to the fact that the graphite from EVs' LIBs destined to the recycling process is not enough in order to fill the natural graphite lacks, thus it is necessary an increase of synthetic graphite in the anode mix.

From scenario C (dashed and continue light green lines, Figure 41), in which all the graphite is recycled but just the 5%, 10%, 15%, and 20% of the required graphite progressively through 2022, 2032, 2042, and 2050 comes from the recycling process, it is possible to observe that the production of recycled graphite follow the same trend as scenario B (dashed line), but just as regards the recycled graphite for LIBs the trend follow much lower values (continue light green line) reaching only less than 1500 kt of recycled graphite for LIBs in 2050. This trend can be observed even from bar diagram (Fig. 42) in which are plotted the total produced recycled graphite of scenario C, that is split into produced recycled graphite for LIBs (light green), and recycled graphite for other industries (dark green) for the years 2022, 2032, 2042, and 2050.

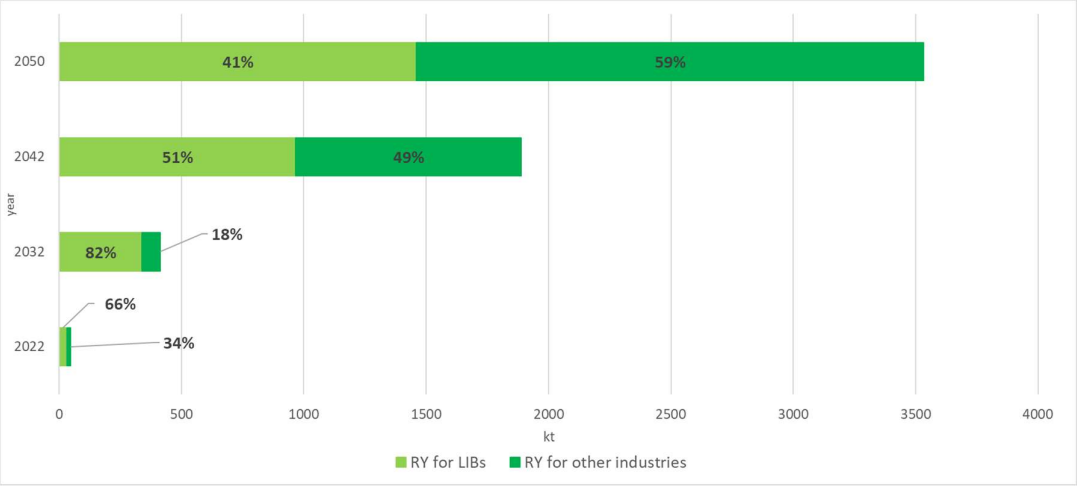

Figure 42. Scenario C, bar diagram, dark green: produced recycled graphite (TOTAL), light green: recycled graphite for lithium-ion batteries, light blue: recycled graphite for other industries.

Figure 42 shows that in 2050 just the 41% of the produced recycled graphite is used for LIBs. In addition, it is possible to notice how the percentages of recycled graphite used for LIBs changes in 2022, 2032, 2042, and 2050, which are respectively 66%, 82%, 51% and 41%. This variation toward lower values could be related to the output values shown in

Table 3, in which it is possible to notice that the EOL vehicles (outflow) will increase a lot up to 2050 (0.955 million in 2022, 8.23 million in 2032, 37.57 million in 2042, and 70.34 million in 2050), and thus the percentages suggested by the scenario (5, 10, 15 and 20%) don't follow the EVs' EOL growing trend in an optimal way. The availability of graphite from EOL EVs will increase exponentially up to 2050, and as explained previously, scenario C takes into consideration that the percentages graphite necessity that come from the recycling process are 5% in 2022, 10% in 2032, 15% in 2042, and 20% in 2050. From the results it is clear that these percentages are not proportional to the rapid increase of EOL EV, and thus to the potential increase of produced recycled graphite.

Finally, as regards scenario D, from Figure 41, it is possible to observe that the produced recycled graphite has lower values during most of the path, but the last values are almost the same as the other scenarios. This is caused to the fact that in this scenario, not all the graphite is destinated for the hydrometallurgical process, this scenario reflects more what could happen in a global level because it is not possible to agree all the countries in the world to recycle all the graphite from anode of EVs' LIBs. This process will be slow as the "produced recycled graphite" line shows.

5 Discussion

5.1 Mineral Analyses

From the SEM pictures it is possible to observe that there are some differences between the three final products, i.e. Natural Graphite, Synthetic Graphite, and Graphite After Recovery. The first sample has a potato shape (Fig. 8), while the second one has more angular and layered shapes (Fig. 11) and the third and last one has soft-angular morphologies (Fig. 21). The motivation of these differences could be explained by the fact that the Natural Graphite sample is not subjected to the graphitization process, and thus the result of the shape milling process (round particle formation) is not altered by the graphitization (crystallization). Instead, the Synthetic Graphite sample is generated by Green Coke, which has a strong angular shape (Fig. 9) and after the shape milling process it must be graphitized. Thus, the previously formed round particles will have a different morphology caused by the redistribution of the carbon atoms in a more ordered structure (Fig. 1). With regard to the graphitization process, from Fig. 13 it is possible to observe the encrustation of the graphitization residues with their preserved morphologies, which varies between semi-ramified crusts, round-crust structures, and cauliflower structures and

this morphological variation could be caused to the different temperature deposition of the residues: the graphitization process has a duration of approximately one week, and it consists of a slow heating of the milled coke, the attainment of a plateau temperature, and then a slow cooling. In theory, the graphitization residues should be composed by the impurity elements of the green coke sample, as S, Mg, Ca, Si, Fe shown in Table 7, while from the graphitization residues EDS the impurities are Ti, V, Ni, and W. This difference in composition depends on the fact that the EDS analyses are performed in one selected point and not in the whole sample surface, in addition the analysed samples come from a huge batch, but the composition can change from one zone to the other of the batch. From the EDS analysis, it is possible to observe that the darker zones correspond to higher pure carbon content while the whitest ones are characterized to the presence of oxides of carbon and titanium.

For the Graphite After Recovery the situation is different. Even in this case, the material doesn't pass through the graphitization process because the starting material is already graphite. Fig.17, which illustrates the SEM pictures of the Graphite Before Recovery, shows that the layered structure of the crystal particles is present, but even more angular shapes and smallest and whitest (Figures 17 and 18) particles which are impurities, as the EDS analysis (table 12) shows. Then, after the purification, these features, except for the layered structure, disappear (Figures 19 and 20, table 13), save for some little impurity as S, Na, and Si. The SEM-EDS of the final product (Graphite After Recovery sample, Figures 21 and 22, and table 14) shows an improvement on edges and grain size: the particles are more rounded and more homogeneous in terms of grain size (between 10 and 20 μm).

From a crystallographic point of view, the three sample of graphite final products are very similar, and this is clear from the XRD analysis of the Graphite After Recovery, Synthetic, and Natural (Fig. 24). All the peaks correspond to the ones of the standard graphite at both phases (2H and 3R). There is only one exception for one peak at 43.5 2θ for the Natural Graphite sample, which shows the presence of another 3R phase in the sample. As regards the recycling processes, the XRD analysis of the Graphite Before Recovery, After Purification, and After Recovery (Fig. 23), show that there is a substantial difference in crystal phases between Graphite Before Recovery sample and the After Purification and Recovery samples. In particular, there are a lot of peaks from 5 to 39 2θ in the black line which suggest the presence of different mineral phases inside the sample caused by the

presence of the impurities showed from the XRF analysis (Table 18). These impurities decrease thanks to the thermal treatment for the purification of the EOL graphite.

The XRF analysis of the graphite samples of the Graphite Before Recovery, Graphite After Purification, and Graphite After Recovery, show their evolution of the chemical composition through the recycling process. The starting product is graphite from EOL batteries, which has a lot of impurities. The presence of alumina, manganese, and phosphorous is related to some cathode contaminations, while the copper is attributable to some collector residues, and silica to insulation components of the EV batteries. The other elements as calcium, iron, potassium, sodium, and titanium are linked to the fact that the graphite used for the batteries is a mix of synthetic and natural and it is possible to observe that these elements are present even in the XRF analysis of the Synthetic Graphite and Natural Graphite samples (Tables 16 and 17). The impurities of Natural Graphite and Graphite After Recovery samples are well indicated from the backscattered electron pictures (BSE) (Figure 22) and from the EDS analysis (Tables 6 and 14), in fact, the Natural Graphite BSE pictures show some little and white particles which are oxidized graphite particles with Na, Mg, Al, Si, Ti, and Zr. The Graphite After Recycling BSE picture shows one single white particle with 3.25% of tungsten, although I suppose there are more than one impurity particle. As regards the Synthetic Graphite sample, there are no evidence of impurities from the EDS analysis, but I think that this is related to the fact that the sample comes from the purest site of the batch. In addition, this can be caused to the different kind of analysis performed by the EDS, which is punctual, and it doesn't take into account the whole sample.

From the TEM analysis it is possible to observe that the atomic structure of natural graphite, synthetic graphite and graphite after recovery samples present different features. The TEM analysis of the natural graphite sample shows that the roundness of the particle is the result of the rolled structure of the macro-graphite layers (Fig. 26), and this arrangement could be caused by the shape milling process. With regard to the atomic structure, the natural graphite sample presents some discontinuity and deformation (Fig. 28) that could be caused by the milling processes, but what is relevant is that the uniformity of the crystals shows that the sample is compact and that the deformations are well integrated with the crystal structure.

Instead, the synthetic graphite TEM analysis shows that the internal structure of the selected particle is composed by different parallel macro layers, which are visible thanks to their dark colour lines alternated by whitest layers that are empty zones, white because of the complete electron transmission of the zone (Fig. 30). The regular and ordered macro structure can be caused to nature of the starting product, which is green coke that crystallize during the graphitization process, after the impact and shape milling. For this, the probable disordered structure of the green coke after the milling processes could have been rearranged by the crystallization of the carbon atoms. Even in this case, as for the natural graphite, it is possible to observe some deformation zones, but from Figure 31, at magnification of 13k X, it is possible to observe that the deformations are well integrated to the graphite atomic structure, and this is visible thanks to the soft lines that characterize the deformation zones. The soft deformation lines could be associated to the transition between coke and graphite, in particular, I suppose that these visible streaks could be the crystallization of deformation zones formed during the milling processes, and probably, the graphitization process didn't last long enough to form a crystalline atomic arrangement. As regards the graphite after recovery sample, the selected particle presents an internal structure made of rolled macro layers (Fig. 34). This characteristic appears even in the natural graphite sample (Fig. 26), while the synthetic graphite one presents parallel and ordered macro layers (Fig. 30). This feature can be associated to the fact that the after recovery and natural graphite samples are already graphite at the beginning of their purification process, thus the roundness given by the shape milling process and pre-processing has not been modified by the graphitization process. In addition, the graphite after recovery sample presents several slips and discontinuities visible thanks to the alternations of dark and white layers (Fig. 34 and Fig. 35). At the magnifications of 8 kX and 12k X it is possible to observe that the slip zones are not a simple fracture, but a stripe with an ordered atomic structure but with different orientation compared to the nearby zones (Fig. 36 and Fig. 37). These discontinuities and fractures could be the result of the entire recovery process starting from the battery dismantling, in which the batteries are crushed, and the graphite is separated by hydrometallurgical process to the rest of the metals present in the cathode and anode, in addition, another contribution to the fractures and discontinuities could be caused by the action of the pre-processing.

5.2 Material Flow Analysis

From the actual global climate crisis and by the geopolitical recent events, two important goals are to reduce the human activities' environmental impact of any kind, and to reduce the economic dependence of Europe from the rest of the world. The growing EV's demand implies an increment of material demands, including graphite for lithium-ion batteries. Today, graphite for LIBs is composed by a mix of natural and synthetic graphite, and this last one is produced by petroleum coke. More specifically, the starting product of the synthetic graphite is petroleum coke produced by delayed coking of petroleum refinery residues, which is crushed, shape milled and heated in order to get round graphite particles. The main producers and holders of natural graphite are respectively China, Brazil, Mozambique and Turkey, China, Brazil and considering that the main petroleum producers are United States, Russia, and Saudi Arabia (*U.S. Energy Information Administration, 2021*), it is clear that Europe does not hold a position in the primary sector. For this reason, it is important to understand which scenario fits with the two goals of economic independence and reduction of environmental impact.

The baseline scenario, compared against the others, shows that the demands up to 2050 of natural and synthetic graphite are lower than those of the of synthetic graphite for the other scenarios, in which it was assumed that natural graphite is replaced by the recycled one in the EVs' LIBs production. The results show that even if all the graphite from LIBs is recycled (scenario B, "100% recycled and used"), there wouldn't be enough to cover the natural graphite lack, or at least, it could be possible to reach the same values as natural graphite of baseline scenario only in 2050 (Fig. 40). This implies that the production of synthetic graphite must be increased almost twice with respect to the baseline scenario values up to 2050, when the recycled graphite production can reach the same values as the natural graphite.

The substitution of recycled graphite to the natural one is a big advantage in order to avoid air and soil pollution and health and social diseases likes heart and respiratory problems (*Whoriskey et al., 2016*, and *Zhang et al., 2014*) caused by graphite mining. On the other hand, according to the previous observations, at least until 2050 the link between electric vehicles and petroleum is stronger than the option of the baseline scenario, in which recycling is not taken into consideration.

In order to avoid the increase of coke demand for the synthetic graphite production, it could be interesting to take into consideration a mix of synthetic, natural and recycled graphite

at least up to 2050. By this way, thanks to the inclusion of natural graphite in the mix, it is possible to control the synthetic graphite demand, and thus the coke necessity. This solution may be effective to avoid the increase of petroleum dependence of the graphite for LIBs, but on the other hand it delays of about 30 years the distancing of the link between EVs' LIBs and mining.

The analysis of the scenarios with the recycling option shows that scenario B ("100% recycled and used") and C ("100% recycled, gradual use for LIBs") produce the highest kt of recycled graphite, but just in scenario B directs the 100% of them to the LIBs for EVs market, while in scenario C, only a little growing percentage up to 2050 of graphite demand comes from the recycling process, the remaining recycled graphite is directed to other industries. Instead, as regards scenario D ("gradual recycling, 100% for LIBs"), the produced recycled graphite is lower than the other scenarios, but when the year 2050 is reached the production of all three scenarios is the same (Fig. 41)

Scenario C considers the options that not all the recycled graphite has the quality as the natural or the synthetic ones, and that not alle the EV companies are ready to use recycled graphite. Scenario D considers the fact that not all the graphite from EVs is ready to be recycled. In any case, the two scenarios take into consideration that the transition to the use of the recycled materials will not be immediate.

Considering that any kind of transition requires time, it is most probable that the future of the use of recycled graphite in the EV market will be a mix of scenario C and D. The transition towards a global use of EVs will be slow in all aspects, from the LIBs' graphite that can be recycled to the recycled graphite for the EVs' LIBs. These aspects can be caused to the fact that not all the graphite from EVs can be recycled and not all the recycled graphite will be used for the EV market. Therefore, the mix of scenario C and D well reflects a slow coordination between states and companies for a E-transition.

Observing even scenario B, it is evident how this scenario is the best way to have a transition towards the use of recycled graphite. The implementation of scenario B in the future of the LIBs could be possible thanks to state legislation governed by global regulatory which require the use of recycled material, where possible, in the EV market.

Finally, In this work I do not present data on CO_2 emissions caused by coke and pitch production, synthetic graphite production, natural graphite mining and purification, LIB and EV production, and graphite recycling process. However, what is clear is that the link between EVs' LIBs and petroleum and mining is strong, and at this point, if the recycling can weaken this bond, it is important to improve and accelerate its entry into the market.

5.3 Innovative aspects (EIT chapter)

In this master thesis I attempt a combination of MFA and mineral analysis to elaborate a critical forecast of the future of graphite recycling and its circularity into Li-ion batteries for the electric vehicles market.

This combination shows that the mineral analyses help to understand better the production processes and the chemistry of the material in exam making the entire work whole. From these two methodologies, it is possible to observe that the use of recycled graphite is possible and that the complete use of recycled graphite instead of the natural one can be complete by the 2050. Therefore, in 2050 it will be possible to use recycled graphite together with the synthetic one, which implies that the natural graphite market can be abandoned.

In order to deal with this master thesis project, I had to analyse and understand the actual and future global approach to the electric vehicle sector and to challenge the sustainability of the it if the entire world will use EVs and if, using three different scenarios, the graphite of EVs' lithium-ion batteries will be recycled (OLO 1). In addition, the baseline and the results of this master thesis project have been possible thanks to the preliminary research, to the study of the synthetic and recycled graphite processes in Elkem Vianode, and of course thanks to the research for the interpretation of the obtained data (OLO 5). The mineral analysis interpretation is the result of the combination between chemical and morphological observations and the application of the synthetic, natural, and recycled graphite system knowledges obtained during the internship in Elkem Vianode (OLO 3)

6. Conclusions

The rolled internal structures and the similar composition of natural and recycled graphite suggest that the substitution of the natural one with recycled one is possible but observing the several fractures and discontinuities in the recycled graphite sample, it is possible that the efficiency of it can be compromised. The limitations of these deformations could be indeed the obstacles that the lithium ions can encounter during the migration, but the rolled internal conformation of the macro layers can help to avoid the structural obstacles.

Considering all the analysed features of the different samples, the substitution of natural graphite with the recycled one could be possible, but it is probably necessary to improve the dismantling and recycling process in order to avoid an excessive fracturing of the particles. In addition, for the future studies, in order to understand the purity and the

effective efficiency of the natural, synthetic and recycled graphite, it could be interesting to determine the carbon content by Loss-on-Ignition (LOI) test (from Jara et al., 2020), the formation of the materials Solid Electrolyte Interphase layer (SEI) by First Cycle Efficiency, and the materials capacity losses by Reversible Capacity tests.

The penetration of electric vehicles is increasing thanks to their lower CO_2 emissions compared to internal combustion engine vehicles, despite this, it is important to further reduce emissions by control of the LIBs' material production and the use of it. The production of synthetic graphite is strictly connected to the petroleum production since the starting product of the synthetic graphite production is petroleum coke, produced by delayed coking of petroleum refinery residues, while the natural graphite production and since natural graphite has big consequences on a humanitarian and environmental level because of the graphite dust in the mine surrounding area (*Whoriskey et al., 2016* and *Zhang et al., 2014*). The introduction of the use of recycled graphite in EVs' LIBs market, in place of the natural one, is a big advantage at least to contrast part of the pollution caused by the graphite mining, but on the other hand, until 2050, the increasing LIB demand leads to an increase in synthetic graphite demand, that cannot be limited by recycling due to the limited amounts of battery scrap available, and thus the bond between petroleum and graphite is increasingly tight. To counteract this trend towards highest demand of synthetic graphite, and thus, coke, I suggest to consider to meet the graphite demand by reconsider to use the natural graphite in order to fill the lacks caused by the poor availability of graphite scraps. By this way, the synthetic graphite demand doesn't increase, while the natural graphite demand will decrease up to 2050 thanks to the growing recycled graphite production by the 2050.

Further research could study how a decrease in petroleum production due to various geopolitical, environmental, and economical factors may influence the synthetic graphite production. In addition, it could be interesting to introduce the production bio-coke in the system as a substitute from petroleum-based coke, as described by Huang et al. (2018). Another suggestion for the next studies is to study another input of graphite for recycling that comes from other E-devices with lithium-ion batteries, like portable electronic devices, in addition to the electric vehicles. By this way, it is maybe possible to increase the produced recycled graphite and decrease the synthetic graphite demand for the first years up to 2050. Lastly, another study could be carried out on where are the main EVs

producers and where are the main EV landfills, that, by following the logic of my thesis, are the future mines of this industry, both for the graphite recycling and for the recycling of the other components. In addition, the combination of the two methodologies of mineral analysis and Material Flow Analysis proved to be complementary. In particular, structural and chemical analyses help to understand better the quality and composition of the material in exam, and to understand better the function of each single process.

Acknowledgements

I would like to thank professors Paolo Garofalo (University of Bologna), and Daniel Beat Müller (Norwegian University of Science and Technology), and the PhD students Fernando Aguilar Lopez, Romain Guillaume Billy (Norwegian University of Science and Technology) for their time, hospitality, and helpful suggestions.

Thanks to Gunstein Skomedal, Bridget Catherine Deveney, Jose Paulino Peris Sastre, and the rest of the Elkem Vianode team for providing me the essential data for the construction of this master thesis and thank you for hosting and supporting me during the internship period.

In addition, I would like to thank Per Erik Vullum (NTNU) for the help with the TEM analyses, Søren Henriksen (Elkem) for the XRF analyses, Pål Baggethun (Elkem) for the XRD analyses, Anders Hope Amundsen (Elkem) for the help with the SEM-EDS analyses.

Reference list

Abdelbaky M., Peeters J.R., Dewulf W., 2021, On the influence of second use, future battery technologies, and battery lifetime on the maximum recycled content of future electric vehicle batteries in Europe, Waste Management vol. 125, pp.1-9, DOI: https://doi.org/10.1016/j.wasman.2021.02.032

Brunner P. H., Rechberger H., 2004, Practical Handbook of Material Flow Analysis, Lewis publishers a CRC Press Company, p. 14-59, IBSN 1-5667-0604-1

Canada Carbon, 2022, Synthetic graphite, https://www.canadacarbon.com/synthetic-vs-natural graphite#:~:text=Synthetic%20graphite%20for%20these%20batteries,cost%20of%20automotive %20battery%20systems.

Dunn J., Slattery M., Kendall A., Ambrose H., Shen S., 2021, Circularity of Lithium-Ion Battery Materials in Electric Vehicles, Environmental Science & Technology vol. 55, pp. 5189-5198, DOI: https://doi.org/10.1021/acs.est.0c07030

European Commission, Causes for rising emissions, https://ec.europa.eu/clima/climate-change/causes-climate-change_en#ecl-inpage-984

Fernley M., 2020, The Investor's Guide to Graphite, Battery Materials Explained for Battery Materials Review a division of BM Review Ltd, p. 4-13

Fujimoto K., Mochida I., Todo Y., Oyama T., Yamashita R., Marsh H., 1989, Mechanism of Puffing and the Role of Puffing Inhibitors in the Graphitization of Electrodes from Needle Coke, Carbon vol.27, No 6 p. 909-917, DOI: https://doi.org/10.1016/0008-6223(89)90041-9

Han Y., Kim J., Yeo J., An J.C., Hong I., Nakabayashi K., Miyawaki J., Jung J., Yoon S., 2015, Coating of graphite anode with coal tar pitch as an effective precursor for enhancing the rate performance in Li-ion batteries: Effects of composition and softening points of coal tar pitch, Carbon vol. 94, p. 432-438, DOI: http://dx.doi.org/10.1016/j.carbon.2015.07.030

Handl W., 2021, Natural Graphite, Chapter 6.1.4 of Industrial Carbon and Graphite Materials: Raw Materials, Production and Applications, p. 165-171, DOI: 10.1002/9783527674046

Huang X., Kocaefe D., Kocaefe Y., 2018, Utilization of Biocoke as a Raw Material for Carbon Anode Production, Energy Fuels 2018, vol. 32, p. 8537−8544, DOI: 10.1021/acs.energyfuels.8b01832

Ishii T., Kaburagi Y., Yoshida A., Hishiyama Y., Oka H., Setoyama N., Ozaki J., Kyotani T., 2017, Analyses of trace amounts of edge sites in natural graphite, synthetic graphite and high-temperature treated coke for the understanding of their carbon molecular structures, Carbon vol. 125, pp. 146-155, DOI: https://doi.org/10.1016/j.carbon.2017.09.049

Jara A. D., Woldetinsae G., Betemariam A., Kim J. Y., 2020, Mineralogical and petrographic analysis on the flake graphite ore from Saba Boru area in Ethiopia, International Journal of Mining Science and Technology vol. 30, Issue 5, pp. 715-721, DOI: https://doi.org/10.1016/j.ijmst.2020.05.025

Jo Y.J., Lee J.D., 2019, Effect of petroleum pitch coating on electrochemical performance of graphite as anode materials, Korean J. Chem. Eng., vol. 36(10), p.1724-1731 (2019) DOI: 10.1007/s11814-019-0354-3

Kamran M., Raugei M., Hutchinson A., 2021, A dynamic material flow analysis of lithium-ion battery metals for electric vehicles and grid storage in the UK: Assessing the impact of shared mobility and end-of-life strategies, Resource, Conservation & Recycling vol. 167, 105412, ISSN 0921-3449, DOI: https://doi.org/10.1016/j.resconrec.2021.105412

Kershaw J.R., Black K.J.T., 1993, Structural Characterization of Coal-Tar and Petroleum Pitches, Energy & Fuels vol. 7, p. 420-425, https://doi.org/10.1021/ef00039a014

Khan Z. U., Kausar A., Ullah H., 2016, A Review on Composite Papers of Graphene Oxide,Carbon Nanotube, Polymer/GO, and Polymer/CNT:Processing Strategies, Properties, and Relevance, VOL. 55, NO. 6, p. 559–581, DOI: 10.1080/03602559.2015.1098693

Kweku D.W., Bismark O., Maxwell A., Desmond K.A., Danso K.B., Oti-Mensah E.A., Quachie A.T., and Buanya B. A., 2018, Greenhouse Effect: Greenhouse Gases and Their Impact on Global Warming, Journal of Scientific Research & Reports, VOL. 17, p. 1-9, DOI: 10.9734/JSRR/2017/39630

Lee J., Kim W., 2014, Research Trend of Electrode Materials for Lithium Rechargeable Batteries, J. Korean Powder Metall. Inst., Vol. 21, No. 6, 473-479, DOI:10.4150/KPMI.2014.21.6.473

NOAA National Centers for Environmental information, Climate at a Glance: Global Time Series, published April 2022, retrieved on April 15, 2022 from https://www.ncdc.noaa.gov/cag/

Northern Graphite Corporation, 2022, Lithium Ion Batteries, https://www.northerngraphite.com/about-graphite/graphite-growth-markets/lithium-ion-batteries/

Pierson H.O., 1993, Handbook of carbon, graphite, diamond, and fullerenes: properties, processing, and applications, Noyes publications, IBSN: 0-8155-1339-9

Predel H., 2012, Petroleum Coke, Wiley-VCH Verlag GmbH & Co. KGaA, Weinheim, Ullmann's Enciclopedia of Industrial Chemistry, VOL. 26, p. 361-376 DOI: 10.1002/14356007.a19_235.pub2

Robinson R. G., Jr., Hammarstrom M. J., and Olson W. D., 2017, Graphite, Chapter J of Critical Mineral Resources of the United States - Economic and Environmental Geology and Prospects for Future Supply, U.S. Geological Survey, Professional Paper 1802-J, DOI: 10.3133/pp1802J

Rothermel S., Evertz M., Kasnatscheew J., Qi X., Gretzke M., Winter M., Nowak S., 2016, Graphite Recycling from Spent Lithium-Ion Batteries, ChemSusChem vol. 9, pp. 3473-3484, DOI: 10.1002/cssc.201601062

Sawarkar N. A., Pandit B. A., Samant D. S., Joshi B. J., 2007, Petroleum Residue Upgrading Via Delayed Coking: A Review, The Canadian Journal of Chemical Engineering, Vol. 85, p. 1-24, DOI: 10.1002/cjce.5450850101

Sharma S., Patel H.R., Patel K.B., 2020, Comparative study on the carbon–carbon composites developed from petroleum pitch, coal tar pitch, and their mixture, Journal of Composite Materials vol. 54 (23), p. 3395-3404, DOI: 10.1177/0021998320914068

United Nations, 2015, Paris Agreement

U.S. Energy Information Administration, 2021, What countries are the top producers and consumers of oil? https://www.eia.gov/tools/faqs/faq.php?id=709&t=6

USGS, 2022, Graphite (Natural), Mineral Commodity Summaries

West Water Resources, 2021 Graphite Market, https://westwaterresources.net/minerals-portfolio/graphite-market/

Whoriskey P., Chavez M. R., Ribas J., 2 October 2016, In your phone, in the air; A trace of graphite is in consumer tech. In these Chinese villages, it's everywhere, https://www.washingtonpost.com/graphics/business/batteries/graphite-mining-pollution-in-china/, Washington Post

Wombles R. H., Kiser M. D., 2016, Developing Coal Tar/Petroleum Pitches. In: Tomsett, A., Johnson, J. (eds) Essential Readings in Light Metals. Springer, Cham. https://doi.org/10.1007/978-3-319-48200-2_32

Yang X., Torppa A., and Kimmo K., 2021, Evaluation of Graphite and Metals Separation by Flotation in Recycling of Li-Ion Batteries, Materials Proceedings, VOL. 5, p.1-7 DOI: 10.3390/materproc2021005030

Zhang L., Liu X., Wan H., Liu X., 2014, Luobei graphite mines surrounding ecological environment monitoring based on high-resolution satellite data, Multispectral, Hyperspectral, and Ultraspectral Remote Sensing Technology, Techniques and Applications Vol. 92632N, DOI: https://doi.org/10.1117/12.2069232

Appendix

Table 19. Given data of the system processes used for the quantification

Given Data			
No.	**Process**	**Efficiency**	**Abbreviation**
1	Synthetic graphite (SY) production	65%	eff_SY
2	Natural graphite purification	50%	eff_NG
3	Mixing	95%	eff_MIX
4	Punched electrode fabrication	95%	eff_electrode
5	LIBs assembly	100%	eff_LIBfab
6	EVs production	100%	eff_EVprod
7	Use of EVs	100%	eff_EVuse
8	EV dismantling	100%	eff_EVdismant
9	Battery shredding	95%	eff_batt_shredd
10	Separation	95%	eff_separation
11	Pyrometallurgy	100%	eff_PYRO
12	Hydrometallurgy	93%	eff_HYDRO
13	Waste treatment	95%	eff_WT
14	Drying	100%	eff_DRYING
15	Graphite recycling	90%	eff_RY
Abbreviation	**Name**	**Data**	**Unit**
Input_year	EV production in a defined year between 2022 and 2050	See table x	/
Output_year	End of life EVs in a define year between 2022 and 2050	See table x	/
Graph_EV	Graphite in a car	70	Kg
PITCH_SY	Pitch percentage for SY production	10	%
PITCH_NG	Pitch percentage for NG production	12	%
SY_MIX	SY percentage for mixing for the actual scenario	50	%
NG_MIX	NG percentage for mixing for the actual scenario	50	%
Graph_HYDRO	Separated graphite for hydrometallurgical process (between 2022 and 2050)	Variable depending on scenario	%
Graph_PYRO	Separated graphite for pyrometallurgical process (between 2022 and 2050)	Variable depending on scenario	%

RY_LIB	Recycled graphite for LIBs (between 2022 and 2050)	Variable depending on scenario	%
RY_otherEdev	Recycled graphite for other EV devices (between 2022 and 2050)	Variable depending on scenario	
GC_C	Green coke C content	92.5	%
PITCH_C	Pitch C content	60	%
SY_C	SY C content	99.9	%
RawNG_C	Raw natural graphite C content	90	%
NG_C	Purified natural graphite C content	99.9	%
RY_C	RY carbon content	99.9	%

Table 20. Mass balance equations of each process.

Mass Balance Equations			
Process no.	Name	Equation	Value
7	Use of EVs	$(A6-7)-(A7-8)-(A7-0)$	0
8	EVs dismantling	$(A7-8)-(A8-9)-(A8-0)$	0
9	Battery shredding	$(A8-9)-(A9-10)-(A9-0)$	0
10	Separation	$(A9-10)-(A10-11)-(A10-0)$	0
11	Pyrometallurgy	$(A10-11)-(A11-0)$	0
12	Hydrometallurgy	$(A10-12)-(A12-13)-(A12-0)$	0
13	Waste treatment	$(A12-13)-(A13-14)-(A13-0)$	0
14	Drying	$(A13-14)-(A14-15)-(A14-0)$	0
15	Graphite recycling	$(A14-15)-(A15-3)-(A15-0)$	0
3	Mixing	$(A1-3)+(A2-3)+(A15-3)-(A3-4)-(A3-0)$	0
4	Punched electrode fabrication	$(A3-4)-(A4-5)-(A4-0)$	0
5	LIBs assembly	$(A4-5)-(A5-6)-(A5-0)$	0
6	EVs production	$(A5-6)-(A6-7)-(A6-0)$	0
1	Synthetic graphite (SY) production	$(A0a-1)+(A0b-1)-(A1-3)-(A1-0)$	0
2	Natural graphite purification	$(A0a-2)+(A0b-2)-(A2-3)-(A2-0)$	0

Table 21. Model approach equations used for the system quantification.

Variable (flow)	Name	Model approach equation	C%
A6-7	EVs ready for use	$Input\_year \cdot 10^6 \cdot Graph\_EV \cdot 10^{-6}$	98.95
A7-8	EOL EVs	$Output\_year \cdot 10^6 \cdot Graph\_EV \cdot 10^{-6}$	98.95
A7-0	Graphite losses	$(A6-7)-(A7-8)$	0
A8-9	EOL LIBs	$(A7-8)\cdot$ eff_EVdismant	98.95
A8-0	Graphite losses	$(A7-8)-(A8-9)$	0
A9-10	LIB particles	$(A8-9)\cdot eff\_batt\_shredd$	98.95
A9-0	Graphite dust	$(A8-9)-(A9-10)$	98.95
A10-11	LIB particles for pyrometallurgical process	$(A9-10)\cdot eff\_separation \cdot Graph\_PYRO$	98.95
A10-0	Graphite losses	$(A9-10)-(A10-11)$	98.95
A11-0	Evaporated graphite	$(A10-11)\cdot eff\_PYRO$	98.95
A10-12	LIB particles for hydrometallurgical process	$(A9-10)\cdot eff\_separation \cdot Graph\_HYDRO$	98.95
A12-13	Graphite for recycling	$(A10-12)\cdot eff\_HYDRO$	98.95
A12-0	Graphite losses	$(A10-12)-(A12-13)$	98.95
A13-14	Treated graphite <16µm	$(A12-13)\cdot eff\_WT$	98.95
A13-0	Treated graphite >16 µm	$(A12-13)-(A13-14)$	98.95
A14-15	Dried graphite	$(A13-14)\cdot eff\_DRYING$	98.95
A14-0	Graphite dust	$(A13-14)-(A14-15)$	0
A15-3	Recycled graphite for EVproduction	$(A14-15)\cdot eff\_RY \cdot RY\_LIB$	99.9
A15-0a	General losses	$(A14-15)-(A15-0b)-(A15-3)$	99.9
A15-0b	RY for other industries	$(A14-15)\cdot eff\_RY \cdot RY\_otherEdev$	99.9
A1-3	SY for EVs	$((A3-4)/eff\_MIX)-(A2-3)-(A15-3)$	99.9
A2-3	Natural graphite for EVs	$((A3-4)/eff\_MIX)\cdot NG\_MIX$	98
A3-4	Slurry	$(A4-5)/eff\_electrode$	98.95
A3-0	Dust and particle losses	$(A1-3)+(A2-3)+(A15-3)-(A3-4)$	98.95
A4-5	Electrodes	$(A5-6)/eff\_LIBfab$	98.95
A4-0	Solution residues and remanence of electrode foil	$(A3-4)-(A4-5)$	98.95
A5-6	LIBs	$(A6-7)/eff\_EVprod$	98.95
A5-0	Graphite electrodes	$(A4-5)-(A5-6)$	0
A6-0	Graphite losses	$(A5-6)-(A6-7)$	0
A0a-1	Coke	$(A1-3)/eff\_SY$	92.5
A0b-1	Pitch	$((A1-3)/eff\_SY)\cdot PITCH\_SY$	60

A1-0	General losses	$(A0a-1)-(A0b-1)-(A1-3)$	74.59
A0a-2	Natural graphite from mines	$(A2-3)/eff\_NG$	90
A0b-2	Pitch	$((A2-3)/eff\_NG)\cdot PITCH\_NG$	60
A2-0	General losses	$(A0a-2)+(A0b-2)-(A2-3)$	74.8

Ringraziamenti

Vorrei ringraziare i miei genitori per aver sempre creduto in me e nei miei sogni, preoccupandosi sempre di darmi gli strumenti giusti per raggiungerli, questo non mi ha mai fatto smettere di sognare, quindi GRAZIE.
Ringrazio mio fratello per l'esempio che mi ha sempre dato e per i molteplici consigli, ringrazio i miei nonni per l'amore genuino e incondizionato, e ringrazio mio zio per aver creduto nei miei studi.
Ringrazio Matteo per essere stato al mio fianco in ogni momento, sostenendomi, amandomi e dicendo sempre la cosa giusta. Grazie per sostenere le mie ambizioni.
Ringrazio Valeria, Massimo e Davide per avermi accolta, trasmettendomi un senso di calma e pace.
Ringrazio le mie amiche Greta, Alessia, Vittoria, Carlotta e la sesta bimbina Babbo, per esserci ancora dopo 13 anni, grazie per essere la mia seconda famiglia.

Ringrazio tutti voi per avermi dato delle sane e forti radici su cui aggrapparmi, farmi forza e fare sempre ritorno.